Science of the Total Environment 979 (2025) 179461



Contents lists available at ScienceDirect

Science of the Total Environment

journal homepage: www.elsevier.com/locate/scitotenv





Spatiotemporal dynamics of coastal dead zones in the Gulf of Mexico over 20 years using remote sensing

Yingjie Li [a,b,c,*], Zilong Xia [d,e], Lan Nguyen [f], Ho Yi Wan [g,h], Luwen Wan [i,j], Mengqiu Wang [k,l], Nan Jia [a,b], Venkata Rohith Reddy Matli [m], Yi Li [n], Megan Seeley [o,p], Emilio F. Moran [a,q,r], Jianguo Liu [a,b,**]

[a] Center for Systems Integration and Sustainability, Department of Fisheries and Wildlife, Michigan State University, East Lansing, MI 48823, USA
[b] Environmental Science and Policy Program, Michigan State University, East Lansing, MI 48823, USA
[c] Natural Capital Project, Woods Institute for the Environment, Doerr School of Sustainability, Stanford University, Stanford, CA 94305, USA
[d] Jiangsu Provincial Key Laboratory of Geographic Information Science and Technology, Key Laboratory for Land Satellite Remote Sensing Applications of Ministry of Natural Resources, School of Geography and Ocean Science, Nanjing University, Nanjing, Jiangsu 210023, China
[e] Jiangsu Center for Collaborative Innovation in Geographical Information Resource Development and Application, Nanjing, Jiangsu 210023, China
[f] Department of Biological Sciences, University of Calgary, Calgary, AB T2N 1N4, Canada
[g] Department of Wildlife, California State Polytechnic University Humboldt, Arcata, CA 95521, USA
[h] Department of Wildlife Ecology and Conservation, University of Florida, Gainesville, FL 32611, USA
[i] Department of Earth System Science, Stanford University, Stanford, CA 94305, USA
[j] Earth and Environmental Sciences, Michigan State University, East Lansing, MI 48824, USA
[k] School of Remote Sensing and Information Engineering, Wuhan University, Wuhan, 430072, China
[l] Department of Earth Sciences, The University of Hong Kong, Hong Kong 999077, China
[m] Center for Geospatial Analytics, North Carolina State University, Raleigh, NC 27607, USA
[n] State Key Laboratory of Marine Environmental Science, Key Laboratory of Coastal and Wetland Ecosystems (Ministry of Education), College of the Environment and Ecology, Xiamen University, Xiamen 361102, China
[o] School of Geographical Sciences and Urban Planning, Arizona State University, Tempe, AZ 85281, USA
[p] Center for Global Discovery and Conservation Science, Arizona State University, Tempe, AZ 85281, USA
[q] Center for Global Change and Earth Observations, Michigan State University, East Lansing, MI 48824, USA
[r] Department of Geography, Environment, and Spatial Sciences, Michigan State University, East Lansing, MI 48823, USA

* Correspondence to: Y. Li, Natural Capital Project, Woods Institute for the Environment, Doerr School of Sustainability, Stanford University, Stanford, CA 94305, USA.
** Correspondence to: J. Liu, Center for Systems Integration and Sustainability, Department of Fisheries and Wildlife, Michigan State University, East Lansing, MI 48823, USA.
E-mail addresses: yingjieli.edu@gmail.com (Y. Li), liuji@msu.edu (J. Liu).

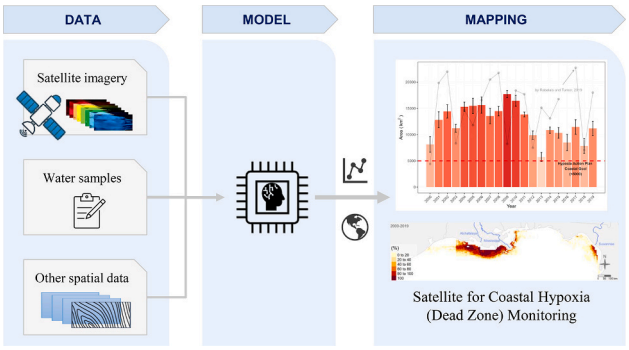
https://doi.org/10.1016/j.scitotenv.2025.179461

Available online 24 April 2025
0048-9697/© 2025 Elsevier B.V. All rights are reserved, including those for text and data mining, AI training, and similar technologies.

HIGHLIGHTS

- Satellite-based models excel in predicting spatiotemporal dynamics of coastal hypoxia.
- We mapped the hypoxia (dead zone) dynamics in the Gulf of Mexico from 2000 to 2019.
- The size and persistence of Gulf hypoxia peaked in 2009 and declined through 2013.
- The 2010–2019 average dead zone was about twice the 5000 km^2 reduction target.
- Our approach is applicable to global coastal dead zone monitoring efforts.

GRAPHICAL ABSTRACT



ARTICLE INFO

Editor: Ouyang Wei

Keywords:
Hypoxia
Eutrophication
Remote sensing
Google earth engine (GEE)
Gulf of Mexico
Coastal sustainability

ABSTRACT

Spreading marine dead zones (or hypoxia) are threatening coastal ecosystems and affecting billions of people's livelihoods globally. However, the lack of field observations makes it challenging to estimate dead zones with spatial precision and across large scales. While satellites offer great potential for detecting environmental changes through large-scale and temporal consistent data, they have yet to be fully integrated into the spatiotemporal dynamic mapping of hypoxia. To address this limitation, we integrated satellite imagery with field observations in random forest models on the Google Earth Engine platform to characterize dead zone dynamics from 2000 to 2019. We applied the workflow to the Gulf of Mexico, which has the largest dead zones in North America. Our model explained 64 % (± 5 %) of the variance in predicting dead zones using satellite data. The analysis revealed that dead zones in the Gulf peaked in 2009 (17,699 ± 679 km^2) and contracted afterward in terms of both size and persistence (% days with hypoxia). Despite this contraction, the average size between 2010 and 2019 was twice that of the coastal reduction goal (< 5000 km^2) set by the Gulf of Mexico Hypoxia Task Force. Furthermore, dead zones occurred more frequently in the western Gulf, and nearly half of the western region experienced dead zones annually. In addition to inter-annual changes, our analysis highlighted the intra-annual dynamics of this phenomenon. Notably, dead zones expanded in June, peaking in size from mid-August to early September. The high temporal and spatial resolution of this dataset allows policymakers to develop targeted management plans and environmental policies. Our approach, which incorporates remote sensing for long-term monitoring of coastal dead zones, can be applied to worldwide monitoring initiatives when paired with local field observations.

1. Introduction

Coastal eutrophication and the emergence of dead zones—defined by hypoxia (oxygen concentrations ≤2 mg/l) and anoxia beneath the water—have increased exponentially over the past half-century (Diaz and Rosenberg, 2008). Globally, over 500 coastal dead zones have been identified (Breitburg et al., 2018), some of which have expanded into mega dead zones (exceeding 5000 km^2, as defined in this study; see Methods), while others, such as the Gulf of Oman, continue to grow rapidly. Yet due to the limited availability of monitoring in many regions, the true number of dead zones may be much higher than currently estimated. This gap in monitoring is critical as more than three billion people depend on marine and coastal ecosystems for their livelihoods (IPBES, 2019). Marine dead zones can result in biodiversity loss and declines in ecosystem services (e.g., commercial and recreation fishing, and tourism) that underpin human well-being (Breitburg et al., 2018). Therefore, it is critical to improve the understanding and prediction of marine ecosystem change at large spatiotemporal scales in order to inform conservation decisions, management plans, and environmental policies that seek to maintain marine ecosystem services.

Traditionally, marine dead zone research and monitoring has been based largely on resource-intensive cruise field observations, which are inherently limited in their spatial and temporal extent (Li et al., 2023b). For instance, in the Gulf of Mexico, cruise hypoxia monitoring across the continental shelf has occurred since 1985 (Rabalais et al., 2010; Smith et al., 2017). In the Baltic Sea, multinational monitoring programs and research cruises have collected water column measurements since 1900 (Carstensen et al., 2014; Conley et al., 2011; Murray et al., 2019). Similarly, dissolved oxygen monitoring in the Adriatic Sea began as early as 1911, conducted by various institutes and projects, with increased monitoring frequency implemented since the 1970s (Brush et al., 2020; Lipizer et al., 2014). The funding and labor resources necessary to monitor these large regions are not adequately available in most coastal regions, leading to either spatially sparse and temporally discrete or nonexistent monitoring (e.g., in the East China Sea (Chen et al., 2007; Zhu et al., 2011)). Further, our comprehension of the dynamics of coastal hypoxia is limited by cruise field constraints as existing studies are often restricted to temporal and spatial extent. Fieldwork campaigns are not only constrained by the costly labor-intensive and time-consuming nature but may also be disrupted by unexpected storms, limited financial and logistical support, and external factors such as pandemics, which have temporarily impacted cruise trips and continuous data collection efforts.

To address this data gap, process-based and statistical hypoxia models have been developed to understand coastal hypoxia patterns and dynamics (Li et al., 2023b). Process-based models use biophysical and biogeochemical processes, including nutrient transport, primary production, as well as water stratification, to predict dissolved oxygen (DO) (Del Giudice et al., 2020; Fennel et al., 2016; Laurent and Fennel, 2019; Obenour et al., 2015; Ou and Xue, 2024; Scavia et al., 2013; Wang and

Justić, 2009). To calibrate and validate these models, site-specific parameter data such as respiration in the water column and sediment oxygen consumption are often required. In many locations, collecting these data is prohibitive to using these models. Statistical models provide an alternative and broadly applicable approach to predicting hypoxia by delineating the empirical-statistical relationship between the size of summer hypoxia zone and factors such as nutrient loads and river discharge (Forrest et al., 2011; Greene et al., 2009; Turner et al., 2012). However, conventional hypoxia statistical models typically focus solely on estimating the total size of hypoxic areas. Consequently, while existing process-based and statistical hypoxia models have advanced our comprehension of coastal hypoxia issues, only a limited number of these models provide spatially explicit information on hypoxia (Justić et al., 2017; Matli et al., 2020).

Earth observation satellites provide an alternative means of acquiring large-scale and consistent data for monitoring environmental changes in both terrestrial and marine ecosystems (Gorelick et al., 2017). For example, satellite remote sensing has been used to map phytoplankton biomass, colored dissolved organic matter load, and sea surface temperature (Le et al., 2014; Zhou et al., 2020). These satellite-derived environment variables can serve as key indicators for predicting dead zones. Long-term remote sensing time series provide valuable opportunities to track historical changes in marine ecosystems and monitor dead zones in real time. However, few studies have utilized these datasets for coastal dead zone monitoring. Notably, Druon et al. (2004) developed a Eutrophication Risk Index (EUTRISK) using satellite-derived chlorophyll-a data from SeaWiFS (Sea-viewing Wide Field-of-view Sensor). While satellite imagery does not directly capture bottom-water hypoxia, this index estimated its potential spatial distribution by integrating bottom oxygen availability with the flux of organic matter reaching the seabed, primarily inferred from satellite-derived chlorophyll-a (Druon et al., 2004). Additionally, Kim et al. characterized the relationship between surface DO and water temperature (Kim et al., 2020). They observed a robust inverse correlation between surface dissolved oxygen and water temperature, highlighting the capability of remote sensing data in modeling surface DO. While this work is promising, hypoxia throughout the water column—particularly at greater depths—is of greater concern than surface hypoxia, as hypoxia at depth is more prevalent and has more severe impacts on marine ecosystems (Rabotyagov et al., 2014; Tomasetti and Gobler, 2020). More recently, Li et al. advanced coastal hypoxia mapping approaches by applying the Moderate Resolution Imaging Spectroradiometer (MODIS) satellite imagery to predict bottom DO (Li et al., 2023b). To date, few studies have applied long-term satellite time series to characterize spatiotemporal dynamics of coastal dead zones.

We addressed this gap in dead zone monitoring by using publicly available satellite imagery and on-site field observations in the Gulf of Mexico. We leveraged the Google Earth Engine (GEE) cloud computing platform to estimate dead zone coverage in the Gulf of Mexico from 2000 to 2019. This timeframe was selected to ensure the availability and alignment of both satellite and field observations. Satellite time series provides a valuable opportunity to assess potential time lags between surface-detectable factors (e.g., phytoplankton blooms, temperature fluctuations) and the onset of bottom-water hypoxia (see Section 2.4.3). By leveraging this approach, our study advances the modeling of spatiotemporal hypoxic dynamics, improving both monitoring and predictive capabilities. Overall, this study advances coastal hypoxia research through three key innovations: First, we integrate satellite remote sensing with machine learning to model hypoxia at unprecedented spatiotemporal resolution, bridging a critical gap in long-term monitoring. Second, our high-resolution mapping captures intra-annual dead zone dynamics, revealing seasonal and episodic patterns often overlooked in coarse inter-annual analyses. Third, we develop a scalable, open-source framework that enables global application, providing policymakers and conservation agencies with a practical tool for rapid assessment and management of hypoxic zones.

2. Materials and methods

2.1. Study region

The Gulf of Mexico, as illustrated in Fig. 1, harbors the most extensive hypoxic zone in North America and ranks as the second largest human-caused coastal hypoxic zone globally. In addition, it was selected as the study area due to the availability of abundant and temporally consistent dissolved oxygen (DO) observations, which are critical for robust model training and validation. The primary cause of hypoxia in the Gulf is the influx of excessive nutrients originating from the human-dominated and agriculturally intensive Mississippi River basin that drains into the Gulf (Pitcher et al., 2021). The Mississippi River basin produces about 80 % of the corn and soybeans, and much of the cotton, rice, sorghum, and wheat in the United States. The heightened intensity of agricultural activity around the mid-20th century coincides with a significant rise in nutrient (e.g., nitrogen and phosphorus) concentrations observed in the Lower Mississippi River (Mitsch et al., 2001). Consequently, the hypoxic zone in the Gulf has been estimated to be as large as 22,000 km^2 in 2008. To mitigate the negative impacts of the hypoxic zone, the federally and state-established Hypoxia Task Force initially set a goal to reduce its size to 5000 km^2 by 2015 (US EPA, 2008). This target has since been extended to 2035 (US EPA, 2023). In this study, we define a hypoxic zone exceeding 5000 km^2 as a "mega dead zone." This threshold was chosen for two reasons: first, it represents a challenging reduction goal for the Gulf of Mexico, and second, it corresponds to the 90th percentile of the size distribution of over 400 global dead zones reviewed by Diaz and Rosenberg (2008).

2.2. Field observations

The coastal water observation data for the 2000–2019 period were compiled from multiple sources including the Southeast Area Monitoring and Assessment Program (SEAMAP) and Louisiana Universities Marine Consortium (LUMCON) (Fig. 2 and Fig. S2). This dataset includes 779,456 samples collected from 150 monitoring cruises at 8117 locations in the Gulf (Figs. 1 & 2). Water sample data include DO measurements, coordinate locations (longitude and latitude), water temperature, sampling date, and depth. The DO measurements were primarily collected using rosette-mounted DO probes by all organizations, except for Louisiana Department of Wildlife and Fisheries (LDWF) and, in some cases, LUMCON. LUMCON primarily utilized hand-held DO probes, in addition to rosette-mounted probes in most years, while LDWF exclusively relied on hand-held DO probes. Detailed data description and data assimilation approach can refer to Matli et al. (Matli et al., 2020, 2018). We filtered the dataset to include only samples collected at depths of 3–80 m, as data beyond this range are sparse in the region and this depth range is typical of the Louisiana–Texas shelf region where hypoxia commonly occurs (Obenour et al., 2013). Additionally, we limited our model development to data gathered between May 1 to September 31 each year, given that hypoxia primarily occurs during the summertime, and most of the water samples were collected within this timeframe (Matli et al., 2018) (Fig. S3).

2.3. Satellite data

We obtained daily MODIS Aqua and Terra Ocean Color level-3 products from May 1 to September 30 during the period of 2000–2019 using Google Earth Engine (GEE). These data included ocean color and estimated biogeochemistry data at the spatial resolution of approximately 4500 m. To predict hypoxia levels, we considered all 14 available satellite-derived variables from the aforementioned MODIS dataset, including ten ocean color bands (412, 443, 469, 488, 531, 547, 555, 645, 667, and 678 nm), three ocean biogeochemical variables (chlor_a – chlorophyll-a concentration, nflh – normalized fluorescence line-height, poc – particulate organic carbon), and sea surface temperature (sst)

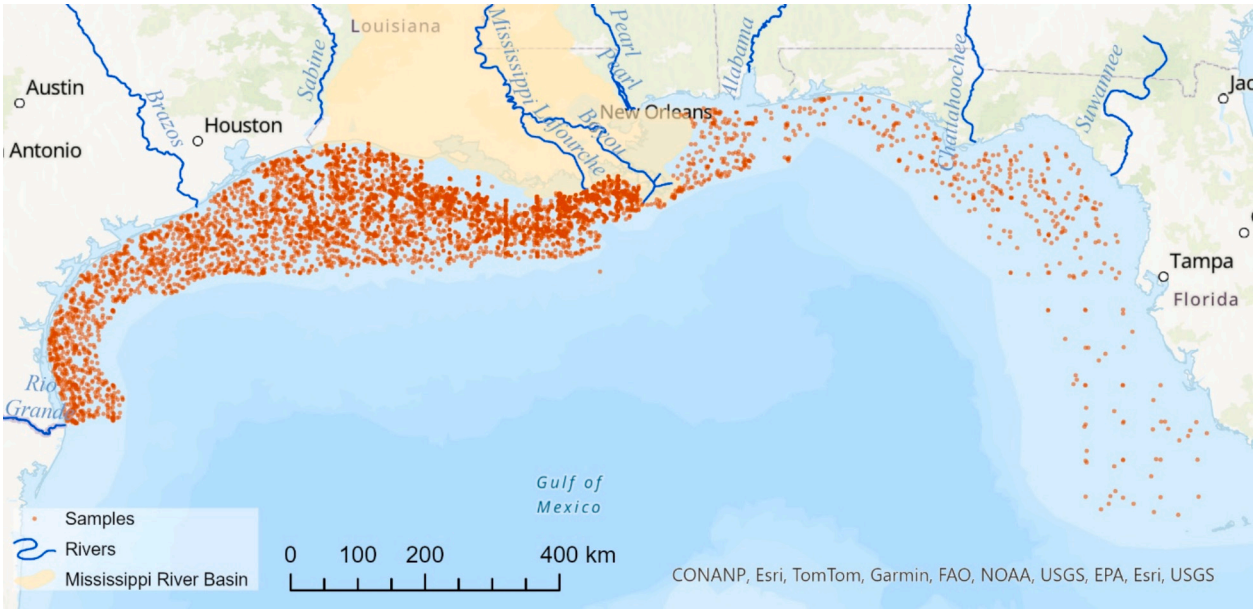


Fig. 1. Geographic distribution of water sampling locations in the Gulf of Mexico.

(Table 1). These variables are considered important factors in modeling coastal hypoxia. For example, seawater temperature can affect water thermal stratification, solubility, and phytoplankton blooms (Jane et al., 2021; Limburg et al., 2020; Turner et al., 2024). While colder water holds more oxygen, thermal stratification driven by density differences can prevent mixing between surface and deeper layers, limiting the transport of oxygen to deeper waters and exacerbating hypoxia. Chlorophyll-a concentration is often utilized as an indicator for phytoplankton blooms, which have the most direct linkage with dead zones (Klemas, 2011; Le et al., 2016; Leming and Stuntz, 1984). In the Gulf of Mexico, hypoxia typically follows coastal eutrophication triggered by the excessive runoff of nutrients from neighboring river basins, particularly the Mississippi River basin. To ensure cloud-free or near-cloud-free and wall-to-wall coverage, we used Terra Ocean Color level-3 products to fill missing pixels in MODIS Aqua Ocean Color level-3 product, and used five-day median MODIS composites as model inputs.

In addition, we also included gridded datasets of wind speed, water salinity, water velocity, and water temperature in the vertical profiles, obtained from NOAA (Cummings and Smedstad, 2013). Wind speed and sea surface temperature are reported to play roles in the biophysical processes controlling hypoxia (e.g., photosynthesis, and stratification) (Altieri and Gedan, 2015; Feng et al., 2012; Jane et al., 2021; Limburg et al., 2020). Salinity influences water density and stratification, which can hinder the mixing of oxygen-rich surface water with oxygen-poor bottom water, thus intensifying hypoxia (Kralj et al., 2019; Rabalais et al., 2010). Water velocity plays a crucial role in either disrupting or maintaining this stratification; faster currents can enhance oxygenation by mixing layers, while slower currents may allow stratification to persist, promoting hypoxic conditions (Allahdadi et al., 2013). We did not include seawater density, because it is determined by temperature and salinity, and gridded data for seawater density is not available. We additionally used gridded bathymetry maps from the General Bathymetric Chart of the Oceans (GEBCO, 2019) to determine the depth of the water bottom. All the gridded data were resampled to match MODIS Ocean Color product resolution. In total, 25 satellite-derived variables were included in the initial analysis (Table 1).

2.4. Dead zone prediction using satellite imagery

To detect dead zones from remote space, it is important to understand the biological phenomena and underlying processes. Although the dead zone formation involves multiple complex biophysical and chemical processes (Fig. S1), it is well-known that, in the Gulf of Mexico, hypoxia is usually preceded by coastal eutrophication driven by nutrient runoffs from the adjacent river basin, especially from the Mississippi River basin. Recent studies also reported climate warming can further fuel the process of blooms and seawater thermal stratification (Altieri and Gedan, 2015; Breitburg et al., 2018; Jane et al., 2021; Limburg et al., 2020). Additionally, warming accelerates heterotrophic respiration and bacterial degradation (Kim et al., 2023; Turner et al., 2024), directly contributing to oxygen depletion in seawater.

2.4.1. Modeling

We used a random forest regression (RFR) model to fit the DO observations with the remote sensing predictors mentioned above. RFR is often used in remote sensing applications as it captures hidden patterns and nonlinear interactions between features in large, complex datasets (Chen et al., 2019; Hutengs and Vohland, 2016). The random forest approach is well-suited for high-dimensional datasets and has been shown to deliver high predictive accuracy (Belgiu and Drăguţ, 2016; Lin, 2017; Teluguntla et al., 2018). In our earlier work (Li et al., 2023b), we evaluated the performance of three modeling approaches—RFR, lagged linear regression, and functional data analysis—for estimating the spatiotemporal variation of hypoxia in the Gulf of Mexico using 2014 data. Among the models tested, the random forest regression outperformed the others in predicting bottom dissolved oxygen from satellite-derived variables. Based on this demonstrated performance, we selected the random forest model for the present analysis to extend the study across a longer time frame and broader spatial scale.

We employed the RFR algorithm integrated into the Google Earth Engine (GEE), enabling us to create a comprehensive workflow within a unified platform. This framework facilitates scalability by allowing other regions to adopt the workflow and integrate region-specific data and parameters to train locally calibrated models (Fig. 3). Remotely sensed data were extracted from each sampling location within a five-day window of when the sample was collected. Following common practice in similar modeling studies (Linderman et al., 2005; Rodriguez-Galiano et al., 2012; Rubí et al., 2023), we randomly chose 70 % of the 8117 field DO measurements (Fig. 1) as training samples, while the remaining 30 % were reserved for model validation. The 70/30 split strikes a balance between providing sufficient data for training the model and retaining enough data to effectively assess its generalization

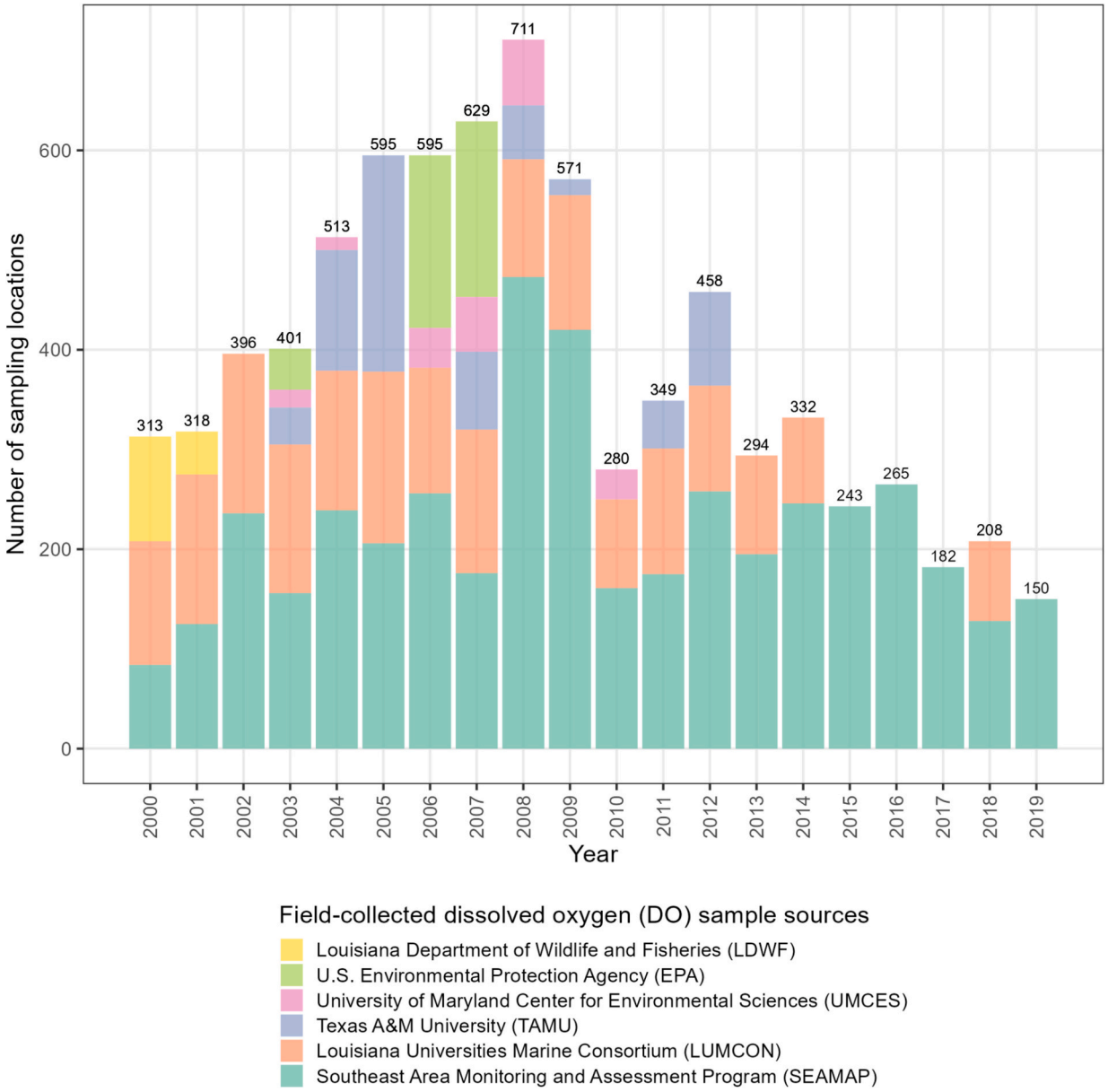


Fig. 2. The number of dissolved oxygen (DO) sampling locations (assuming one sample per location) in the Gulf by year and by collection agency.

capabilities (Rubí et al., 2023). To reduce the risk of overfitting and assess model robustness, we repeated the training-validation process using multiple random seeds ($n = 10$), evaluating model performance across each partition (Li et al., 2023b). We fine-tuned the RFR parameters following established methods (Pelletier et al., 2016; You et al., 2021). This optimization process led to setting the "numberOfTrees", representing the count of binary classification and regression trees, to 99 for our modeling. Other parameters were set as the GEE default. Next, we selected twelve variables for the final model according to the importance score of each input feature (Fig. 4, and Fig. S4) and with consideration of multicollinearity among variables. The importance scores were derived from the RFR model as a calculation of how often predictors were used in trees built by the model. These scores are often used to constrain the number of predictor variables and thereby reduce computational cost and stabilize classification results (Huang and Zhu, 2013; Xia et al., 2022).

2.4.2. Prediction performance

The prediction performance of the RFR models was evaluated using the coefficient of determination: R^2, root mean square error (RMSE), and the mean absolute error (MAE).

2.4.3. Time lags in satellite prediction of bottom DO concentration

As there is likely a time lag between what can be detected on the surface (e.g., phytoplankton events, temperature variations) and hypoxia occurrence in bottom waters beneath the surface (Fig. S1, and Fig. S5), we tested different lag times for our model. Some studies suggest that the time lag between surface water chlorophyll biomass and bottom-water low dissolved oxygen can vary from a few days to more than two months (Chen et al., 2014; Justić et al., 1993; Zhou et al., 2020). Therefore, we investigated time lags from 0 to 80 days (equivalent to two months plus an additional three-week buffer period). To empirically identify the optimal time lag for accurate prediction, we trained RFR models using predictor variables collected at various time lags (0–80 days) where each model included only one time lag. We subsequently assessed model performance at each time lag and selected the time window when satellite-derived predictors exhibited the highest performance to map hypoxia in the Gulf of Mexico from 2000 to 2019.

Table 1
Data sources.

Data description	Variables †	Resolution	Availability	Data source	GEE Collection
MODIS Aqua Ocean Color level 3 product	*chlor_a, nflh, poc, Rrs_412, Rrs_443, Rrs_469, Rrs_488, Rrs_531, Rrs_547, Rrs_555, Rrs_645, Rrs_667, Rrs_678, sst*	4616 m; Daily	2002-07-03 – Now	NASA Goddard Space Flight Center, Ocean Ecology Laboratory, Ocean Biology Processing Group	ee.ImageCollection("NASA/OCEANDATA/MODIS-Aqua/L3SMI")
MODIS Terra Ocean Color level 3 product	The same variables as above, i.e., the MODIS Aqua Ocean Color level 3 product	4616 m; Daily	2000-02-24 – Now	The same as above	ee.ImageCollection("NASA/OCEANDATA/MODIS-Terra/L3SMI")
AVHRR Sea Surface Temperature Climate Data	*wind_speed sea_surface_temperature*	4000 m; Twice-daily	1981-08-24 – Now	NOAA National Oceanographic Data Center	ee.ImageCollection ("NOAA/CDR/SST_PATHFINDER/V53")
Hybrid Coordinate Ocean Model, Water Velocity ‡	*velocity_u_x* (Eastward sea water velocity at a depth of 0–100 m); *velocity_v_x* (Northward sea water velocity at a depth of 0–100 m)	Horizontal: 8905 m; Vertical: 2–5 m intervals at depths of 0–50 m, and 10 m intervals at depths of 50–100 m; Daily	1992-10-02 – Now	National Ocean Partnership Program (NOPP)	ee.ImageCollection ("HYCOM/sea_water_velocity")
Hybrid Coordinate Ocean Model, Water Temperature and Salinity ‡	*salinity_x* (Sea water salinity, in practical salinity units, at a depth of 0–100 m); *water_temp_x* (Sea water temperature at a depth of 0–100 m)	Horizontal: 8905 m; Vertical: 2–5 m intervals at depths of 0–50 m, and 10 m intervals at depths of 50–100 m; Daily	1992-10-02 - Now	National Ocean Partnership Program (NOPP)	ee.ImageCollection ('HYCOM/sea_temp_salinity')
Gridded Bathymetry Data	*Bathymetry*	450 m; No temporal resolution	2020	British Oceanographic Data Centre (BODC)	ee.ImageCollection ("projects/sat-io/open-datasets/gebco/gebco_grid")

† The rationale for selecting variables is detailed in Section 2.3. ‡ For water velocity, temperature and salinity, we used surface values and surface-bottom differences at each location, rather than the full vertical profile.

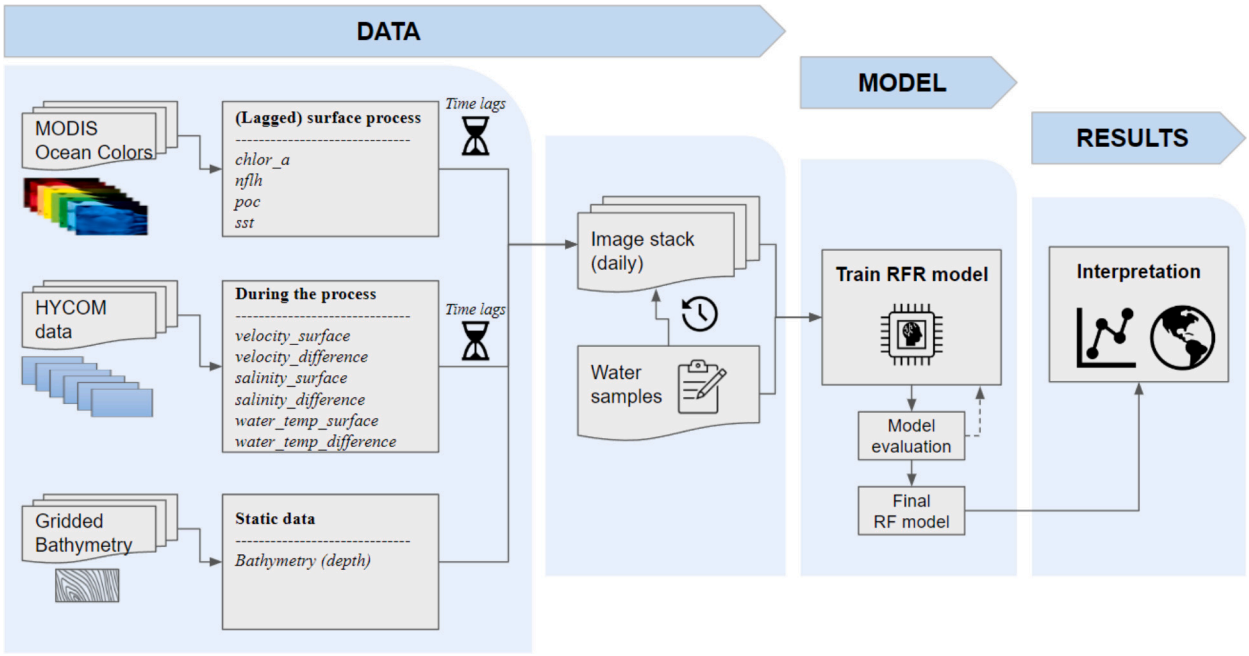


Fig. 3. Workflow for dead zone prediction with random forest regression (RFR) model. Satellite-derived variables from MODIS and the Hybrid Coordinate Ocean Model (HYCOM) were integrated with field-collected water samples by testing a range of potential time lags.

2.4.4. Mapping intra- and inter-annual dead zone occurrence

We define the ***annual maximum dead zone*** as the total area of locations experiencing hypoxia during the summer period (May–September) within each year. This provides an estimation of the total affected area for each year, and allows us to compare our modeled dead zone predictions with those reported by other agencies. To measure the persistence of dead zones each year, we used the ***intra-annual dead zone occurrence*** (DZO_y) to measure the frequency with which dead zones occurred during the summer period each year. DZO_y is computed at the pixel level, as the percentage of the number of days (d) with a detected dead zone (DDZ) among the total days with valid observations (VO) within a certain year (y; Eq. 1). Similarly, we used ***inter-annual dead zone occurrence*** (DZO) to measure the variability in the presence of dead zones across years. Inter-DZO is also computed at the pixel level as the percentage of the total years with detected dead zones (DDZ) relative to the total years with valid observations (VO) over the 20-year period (2000–2019; Eq. 2).

$$DZO_y = \left(\Sigma DDZ_y^d \Big/ \Sigma VO_y^d\right) \times 100\% \quad (1)$$

$$DZO = \left(\Sigma DDZ_y \Big/ \Sigma VO_y\right) \times 100\% \quad (2)$$

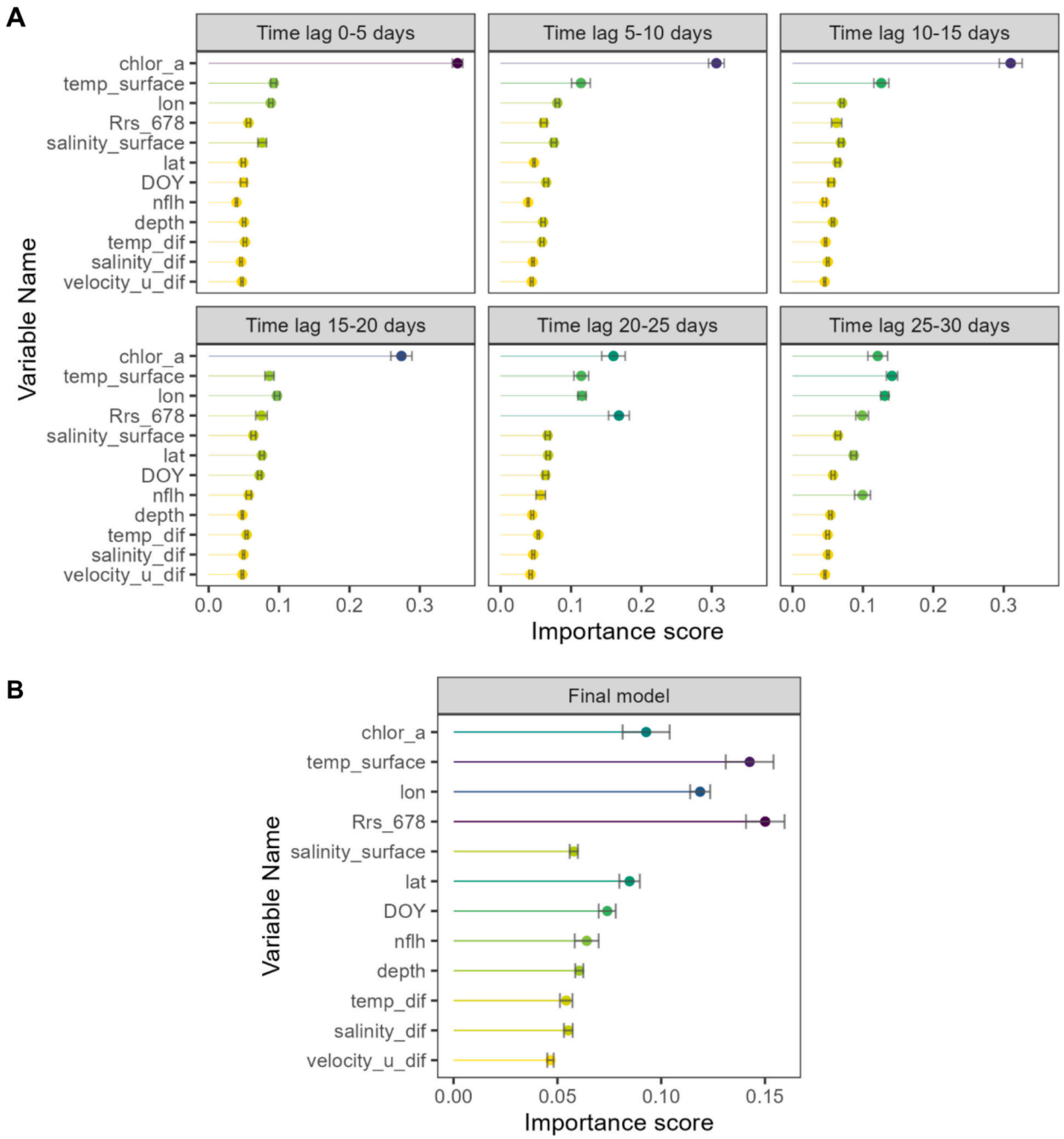


Fig. 4. Importance scores of the selected variables in each lagged random forest regression model (A) and in the final model (B). In (A), each panel presents the results from the models with a range of time lags. For example, the panel named "0–5" shows the average variable importance from models with lagged satellite predictors at 1 to 5-day lags. The error bars represent 95 % confidence intervals. *Temp* – Sea water temperature, *lon* – longitude, *lat* – latitude, *[xxx]_dif* – the difference between values on the surface and bottom water, DOY – day of the year. Refer to Table 1 for all other variable information. See Fig. S4 for the importance scores of all the 28 pre-selected variables (including 25 satellite-derived variables, plus DOY, longitude, and latitude).

3. Results

3.1. Temporal changes of dead zones

Our analysis shows that satellite-derived predictors collected on 30–32 days achieved the most accurate predictions of DO, as this model had the highest R^2 (R^2 = 0.64 ± 0.05) and lowest RMSE and MAE (Fig. 5). Therefore, we chose satellite imagery from these date ranges as model inputs when implementing the RFR for hypoxia mapping. The hypoxic area estimated using this model increased steadily since 2000, peaked in 2009, and subsequently declined through 2013. It stayed at a consistent size of ~10,000 km^2 until 2019 (Fig. 6). Although the dead zone area decreased after 2009, the average size (mean = 11,245 ± 3574 km^2, 2009–2019) continued to exceed the coastal reduction goal set by the 2008 Gulf Hypoxia Action Plan. In most years, dead zones began expanding in June and peaked during mid-August or September (Fig. 7). The dead zones persisted for over three months annually. Since 2011, however, the mega dead zones (area > 5000 km^2) typically persisted for up to one month.

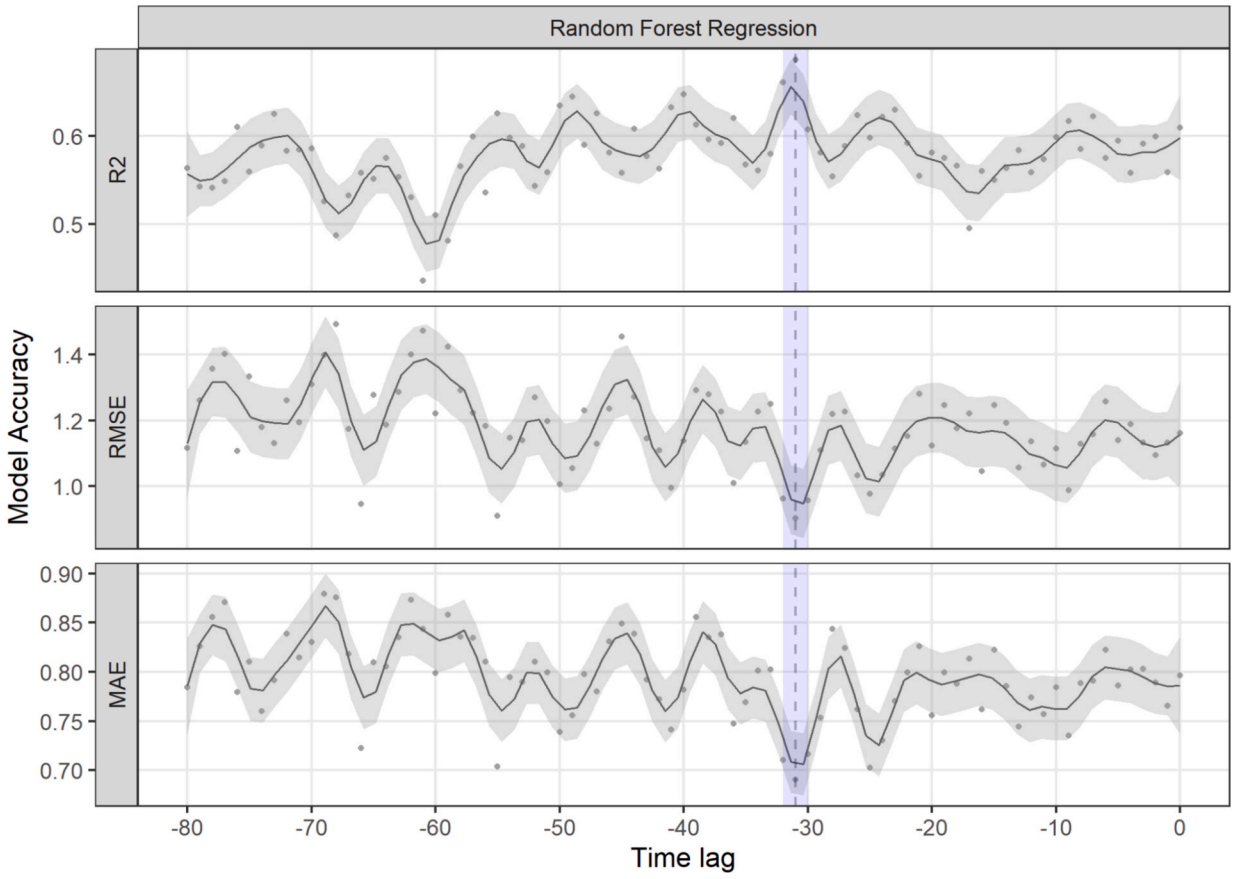


Fig. 5. Model performance for dissolved oxygen (DO) estimation with satellite predictors at different time lags. Model performance is evaluated by R^2, RMSE (mg/l), and MAE (mg/l) between estimated and observed DO. Lines depict mean values, and the gray shades represent 95 % confidence intervals (CIs). The vertical blue shade highlights dates when satellite predictors achieved relatively high accuracy ($R^2 = 0.68$, RMSE = 0.88, MAE = 0.67).

3.2. Spatial patterns

Most dead zones were detected in nearshore waters over the summer. We found that dead zones occurred more frequently (in eight of the 20 years) on the west side of the Mississippi-Atchafalaya Rivers estuary than in other regions (Fig. 8A). Nearly half of the hotspot regions (i.e., the west side) experienced dead zones annually over the 20-year study period. In addition to the northern Gulf region, we also detected dead zone occurrences at the Suwannee River estuary in the eastern Gulf, an area seldom examined in relation to this issue. There is no substantial difference in model performance across different spatial regions (Fig. S6), and 75 % of the testing data points have RMSE <1 mg/l and 94 % are <2 mg/l (mean RMSE = 0.75, sd = 0.63; Fig. 8B).

We further investigated the intra-annual dead zone occurrence each summer from 2000 to 2019 (Fig. 9). Similar to the interannual dead zone occurrence, areas with high intra-annual dead zone occurrence were predominantly found in the northern Gulf region, as well as at the estuary of the Suwannee River (Fig. 9A). The area with over 60 % dead zone occurrence over summertime (or over 3 months) exceeded the 5000 km^2 redline from 2001 to 2012, while the subsequent years were below the line (Fig. 9B). This indicates that the dead zones became both smaller and less persistent after 2012 than in earlier years.

4. Discussion

This study presented the first spatiotemporal mapping of dead zones across 20 years using remotely sensed imagery and machine learning. By introducing and emphasizing the role of satellite imagery in the modeling and prediction of coastal hypoxia, we advanced the approach to monitor and better understand the spatial and temporal dynamics of coastal dead zones. The spatially explicit dead zone maps derived from this analysis unveil both the geospatial attributes of the dead zones in the Gulf of Mexico and their temporal changes across multiple scales, ranging from days to years.

Our results indicate that the Gulf dead zones peaked in 2009 and faded afterward in terms of both size and persistence (measured by intra-annual occurrence). Although the dead zone decreased in size, the average size of these hypoxic regions remains approximately two times larger than the targeted coastal reduction goal of below 5000 km^2, highlighting the critical need for continual management and monitoring efforts. While USGS data indicate a reduced nitrogen application rate from 2012 to 2017 (Falcone, 2021), the reduction magnitude is not substantial (Fig. S6), and likely contributes to the persistence of hypoxic regions over the years.

4.1. Using satellite imagery for dead zone estimation

Our approach using remote sensing provides insight into selecting satellite-derived predictor variables and the appropriate time lags for dead zone prediction. We found the satellite-derived variables can explain 64 % (± 5 %) of the variance in bottom DO, and our model outperforms existing models, which typically explain 41 %–58 % of dissolved oxygen variability (Matli et al., 2020, 2018).

Previous research on dead zone modeling and prediction rarely used satellite data (Matli et al., 2020; Murphy et al., 2011; NOAA, 2022; Scavia et al., 2017; Zhou et al., 2014). Because traditional coastal hypoxia monitoring based on cruise trips is constrained by weather conditions, funding availability, and potential interruption due to unexpected

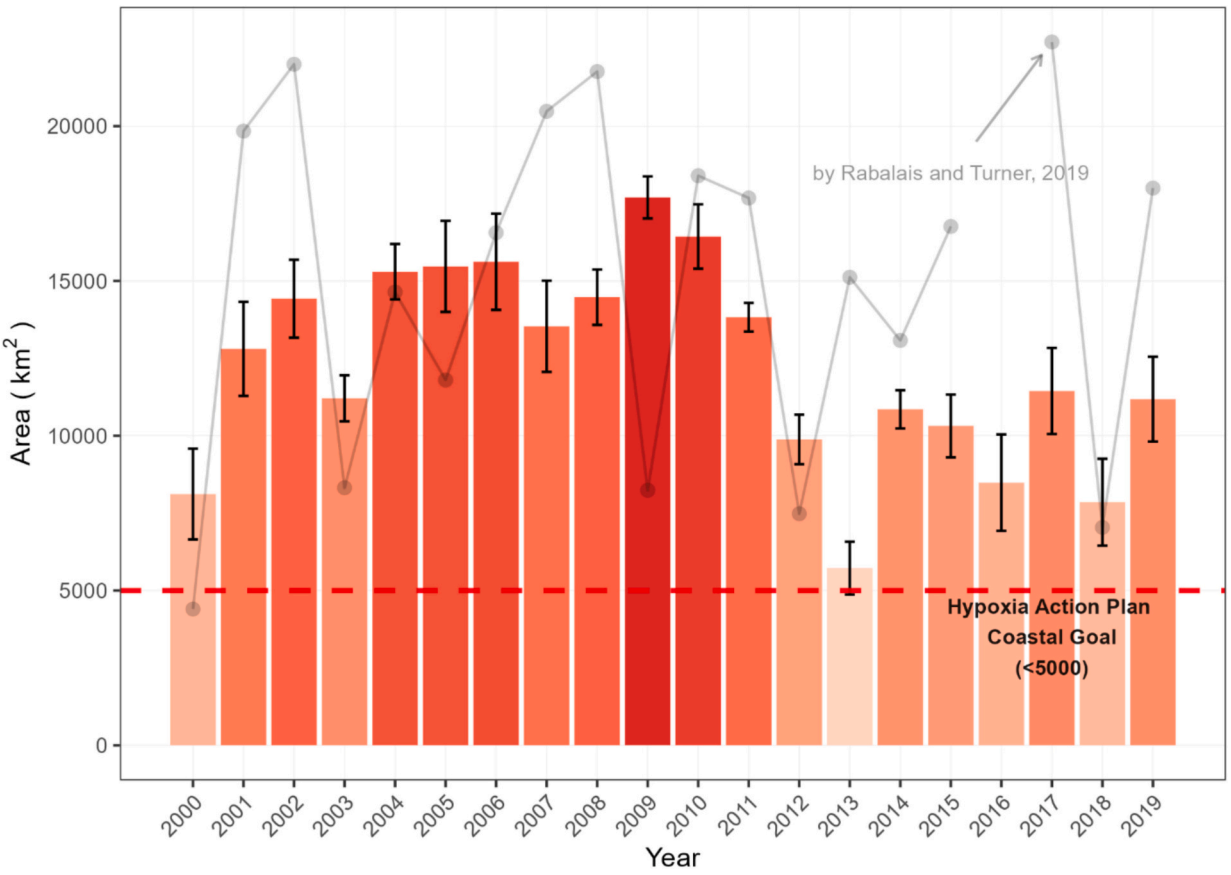


Fig. 6. Annual dead zone area from satellite predictions (2000–2019). Dead zone = bottom water hypoxia (< 2 mg/l of dissolved oxygen). The error bars indicate the standard error of predictions (n = 30 days). Because the area of dead zone changes over time within a year, we used the top 30 maximum daily dead zone predictions during each summertime (when dead zones typically peak) to calculate the standard error of yearly maximum dead zone predictions. The dashed horizontal red line denotes the target of the Gulf Hypoxia Action Plan, aiming to reduce the five-year running average size to <5000 km^2. The light-gray line with dots shows the area of hypoxia (no data for 2016) reported by the Gulf Hypoxia Research Team (see https://gulfhypoxia.net/research/shelfwide-cruises) (Rabalais and Turner, 2019). Please note that the estimation by the Gulf Hypoxia Research Team was based on snapshot data of water measurement and geospatial interpolation approach, which are not strictly comparable to our results.

shocks (e.g., the COVID-19 pandemic), the ground measurements are limited in spatial and temporal coverage, typically providing only a snapshot at a specific time in a year. These constraints further limit the ability to estimate dead zone changes across space and over time. Ocean satellite imagery, such as MODIS and SeaWiFS, can supplement the ground measurements by providing long-term and large-scale information for coastal monitoring. For example, MODIS-Aqua/L3SMI and MODIS-Terra/L3SMI used in this study provide daily imagery since 2000. The SeaWiFS provides satellite ocean biology data dating back to 1997 on a daily basis. However, to maintain consistency, we excluded SeaWiFS from this analysis due to its much coarser spatial resolution (9200 m). Future advancements in data fusion techniques could help integrate such datasets, enabling the generation of more consistent, continuous, and longer-term information to fill data gaps and improve our understanding of coastal processes.

In this study, using 20 years of consistent MODIS satellite imagery, we explored the appropriate time lags between satellite-observed surface seawater characteristics and the occurance of bottom-water hypoxia. Our analysis shows the time lag is most likely at 30–32 days on average. This aligns with previous estimates, such as Zhou et al. (2020), which identified a lag of 1–8 weeks, and Justić et al. (1993), which similarly suggested a maximum lag of 8 weeks. While our findings align with prior studies, there remains an insufficient amount of direct evidence to pinpoint the exact time lag between surface processes and bottom-water hypoxia. The time lag may vary across years due to changes in climate and oceanic conditions. Future studies can use more continuous ground-based measurements (e.g., buoys) and process-based models to better investigate time lag effects.

While satellite data are abundant, they are susceptible to data gaps caused by cloud and sun glint, and inter-orbit gaps. Like most other time-series analyses using remote sensing, our mapping also encountered missing pixel issues in our dead zone mapping (Fig. 10). Those data gaps might lead to an underestimation of the coastal dead zones, even though satellite data provide better spatial coverage than the traditional on-site measurements. Gap-filling using a time series that takes the composite median or mean is the conventional method for addressing these gaps, but it might not be appropriate for detecting time-sensitive changes, such as short-term algal dynamics or dead zone fluctuations on an hourly or daily scale. Further, the fluidity of water may require gap-filling techniques to consider the spatial dimension in addition to the temporal dimension. For instance, some studies have employed soap-film smoothing (Wood et al., 2008) and deep learning-based approaches (Shao et al., 2019), which integrate both spatial and temporal dimensions to address data gaps. Unfortunately, these tools are either currently unavailable on the GEE platform or require additional satellite imagery not available in GEE. Future advances in these techniques and data fusion are expected to address the existing data gaps.

In addition to data gaps in satellite imagery that might limit dead zone mapping, the accuracy and representativeness of satellite-derived variables might also influence model accuracy. For instance, the near-surface concentration of chlorophyll-a, derived from remotely sensed reflectance, serves as a widely utilized proxy for detecting

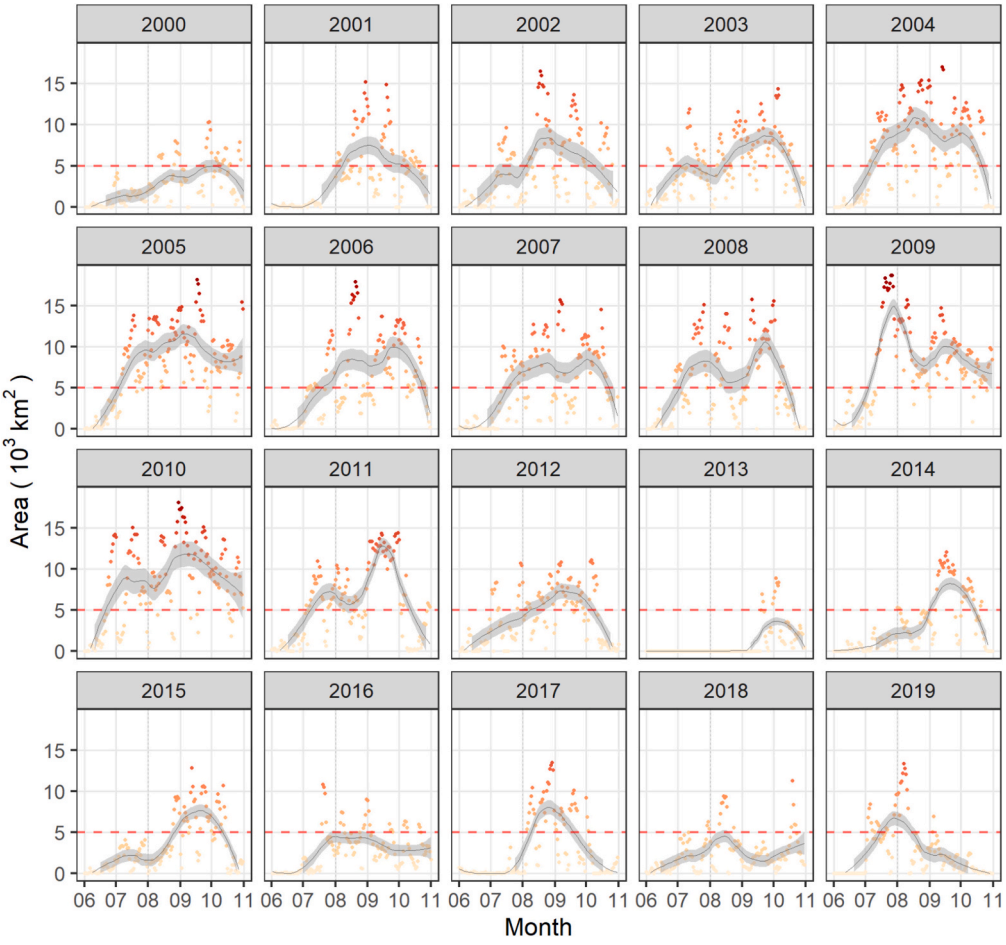


Fig. 7. Intra-annual change of dead zone area over summer months. Dots show the estimated dead zone area each day, and darker red colors indicate larger areas of dead zones. Lines represent the smoothed conditional means using the local polynomial regression fitting method. The gray shades represent 95 % CIs. The dashed horizontal red line denotes the target (< 5000 km^2) of the Gulf Hypoxia Action Plan.

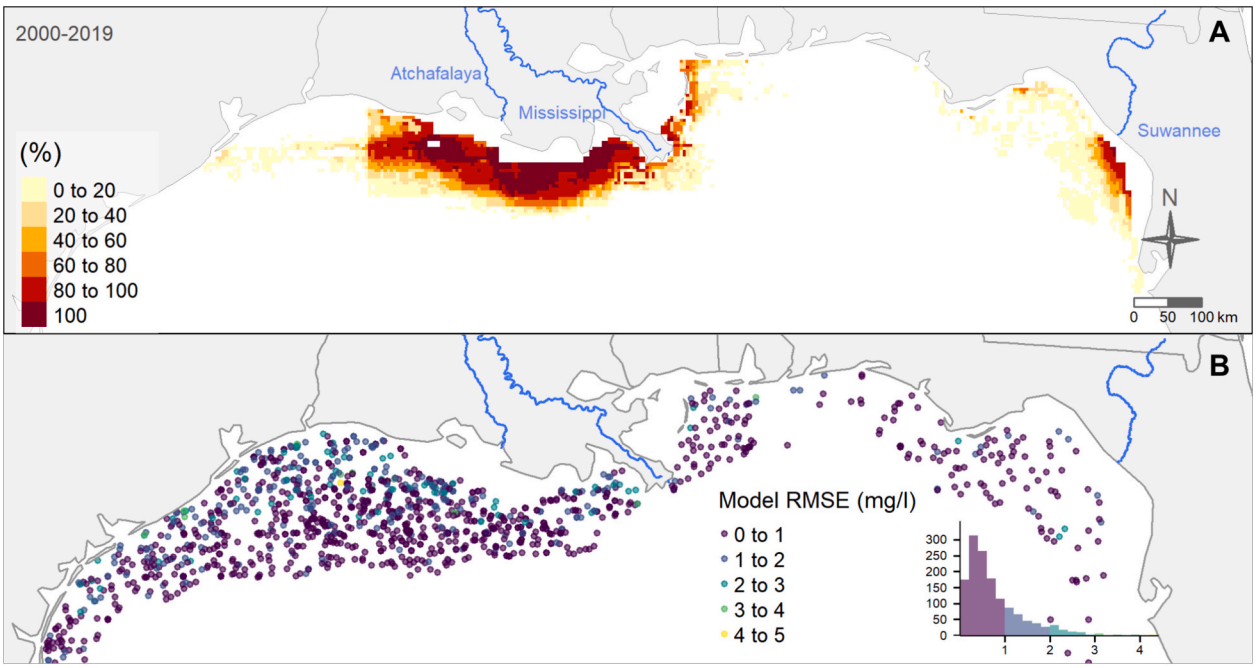


Fig. 8. (A) Inter-annual dead zone occurrence (%) during 2000–2019. All of the colored regions denote dead zone occurrence (dissolved oxygen <2 mg/l). (B) Spatial map of DO prediction performance measured by root mean square error (RMSE; RMSE mean = 0.75, sd = 0.63).

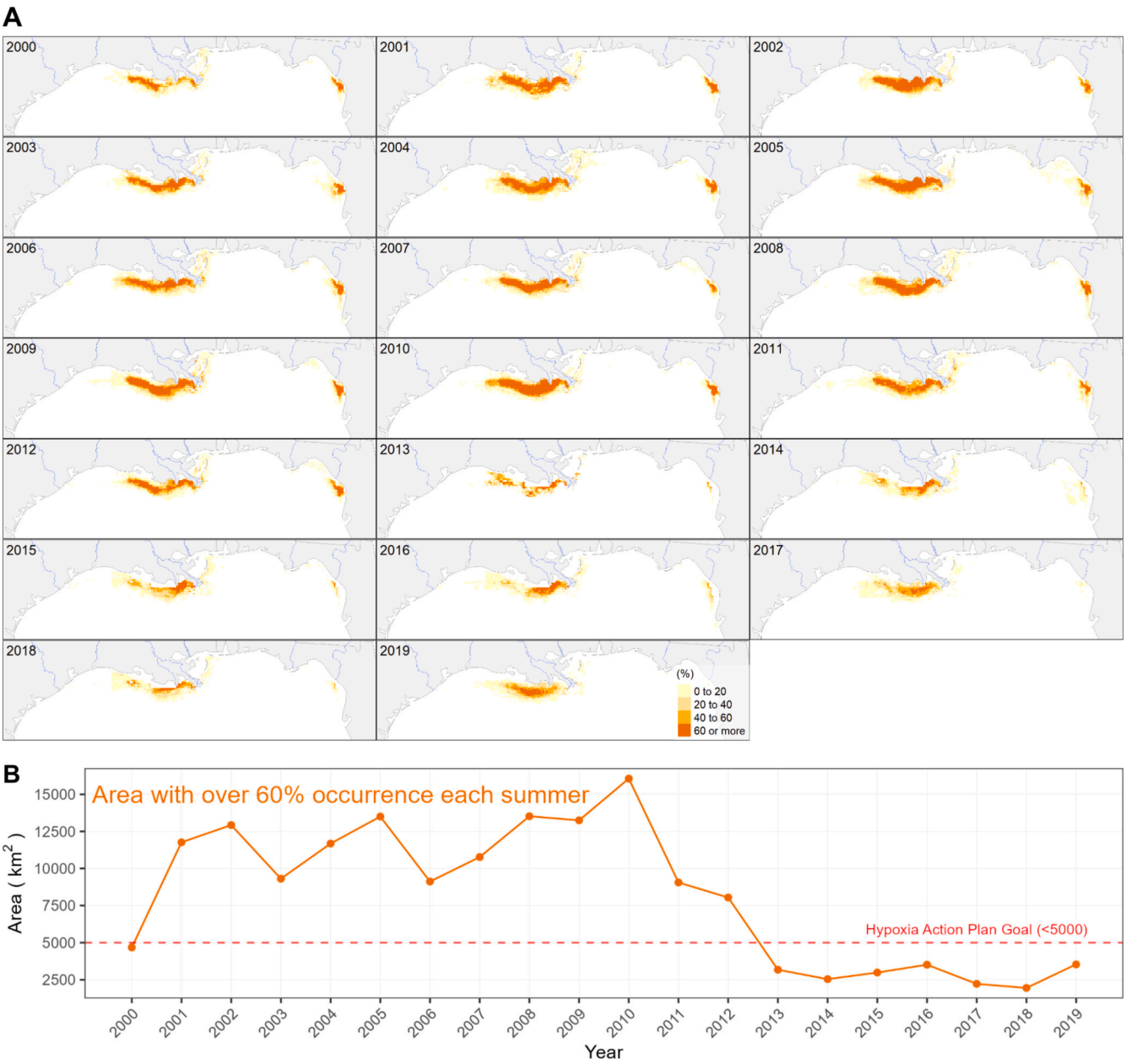


Fig. 9. The intra-annual dead zone occurrence (A), and the size of the area with over 60 % occurrence each summer (B). All the colored regions in A denote dead zone occurrence (dissolved oxygen <2 mg/l).

phytoplankton biomass in open ocean environments (Boyce et al., 2012; Harvey et al., 2015), but these data products include many uncertainties. Taking the chlorophyll-a product by MODIS-Aqua as an example, the mean absolute error (MAE) is about 1.69 mg/m^3 for the global product (https://oceancolor.gsfc.nasa.gov/reprocessing/r2022/aqua/), and the MAE is about 2.38 mg/m^3 for the Gulf of Mexico region when evaluated with in situ observation data compiled by the Gulf of Mexico Coastal Ocean Observing System (https://gisdata.gcoos.org/). Furthermore, different algae species can impact the representativeness of using chlorophyll-a as the key variable for predicting dead zones as not all algae lead to dead zones. For instance, *Sargassum* is considered critical for protecting marine habitats and associated marine species while excessive cyanobacteria, dinoflagellates, coccolithophores, and diatoms in coastal oceans are mainly responsible for causing significant adverse impacts on ocean ecosystems (Campbell et al., 2019). Our model could not distinguish algae genera and thus might lead to an overestimation. Distinguishing the genera will be critical for further improving model accuracy and explanatory power.

Typically, current dead zone predictions rely on hypoxic area estimations from the LUMCON, derived from water sampling during midsummer cruises. We overlaid our predictions with the LUMCON results (Fig. 6) (Rabalais and Turner, 2019) and found that both estimations show similar overall trends, despite some year-to-year variations. The estimations of dead zone areas by LUMCON were largely based on snapshot data of water measurements and geospatial interpolation approaches, which are not strictly comparable to our results. The LUMCON cruise sampling dates were primarily in late July, with some data collected in May and June during the study period from 2000 to 2019. Consequently, it is possible that the measurements missed the timing for capturing important water quality change information. It is therefore important that we integrate discrete ground measurements with continuous satellite observations to construct models and characterize the relationships, enhancing our comprehension of the spatio-temporal dynamics of coastal dead zones. While our satellite-based

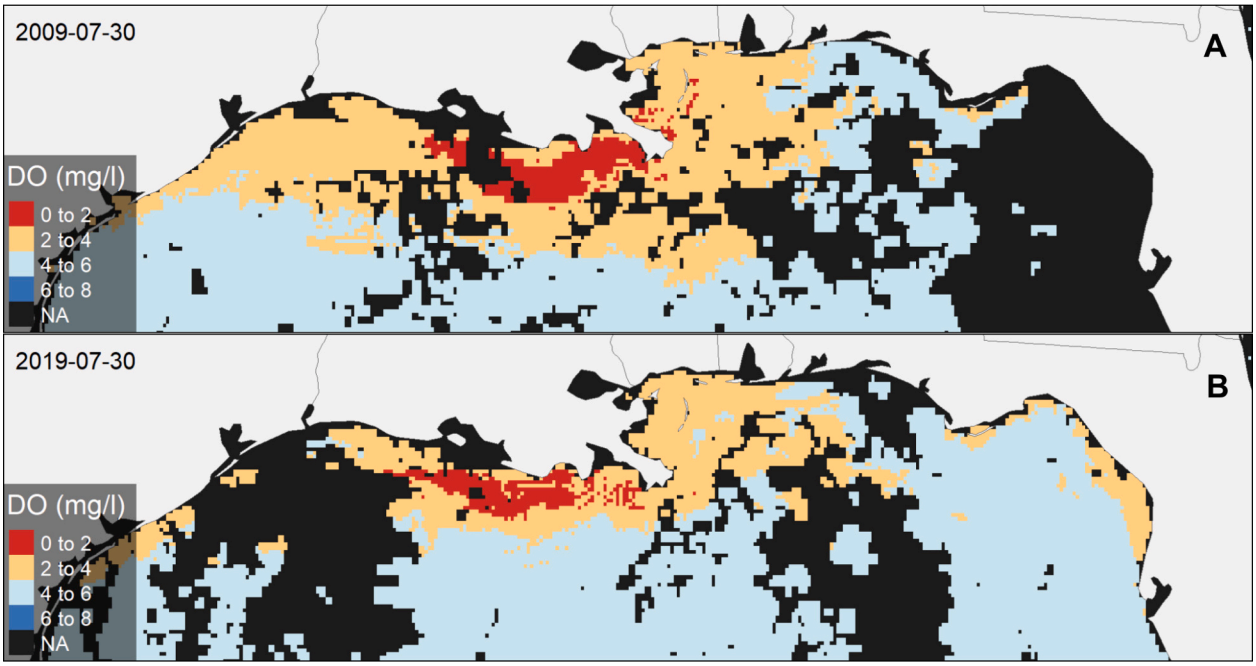


Fig. 10. Predicted dissolved oxygen (DO) levels in bottom waters and associated missing pixel issues. (A) Modeled DO map for July 30, 2009. (B) Modeled DO map for July 30, 2019. Pixels with DO levels below 2 mg/l are categorized as dead zones.

modeling provides valuable reference information for understanding spatiotemporal patterns, it has limitations in capturing the underlying mechanisms driving hypoxic changes. Similarly, field observations, though critical for validation, are spatially and temporally constrained. These challenges underscore the need for continued advancements in validation approaches, including the incorporation of additional in situ data sources and autonomous monitoring systems to improve model accuracy and reliability.

4.2. *Important satellite predictors for dead zone mapping*

Our analysis identified that sea surface temperatures, satellite reflectance at band 678 nm (i.e., the chlorophyll fluorescence emission spectrum), longitude, and chlorophyll-a concentration are the most important predictors in the RFR model (Fig. 4B). This partly aligns with previous studies that demonstrated that phytoplankton events (or their equivalent net primary productivity) and climate warming are two important explanatory variables in hypoxia prediction models (Kim et al., 2020; Le et al., 2016).

Climate warming has become the dominant factor causing phytoplankton events and deoxygenation in both lakes and coasts (Ho et al., 2019; Jane et al., 2021; Kim et al., 2020) as seawater warming can not only facilitate phytoplankton events, water stratification and oxygen solubility (Dagg and Breed, 2003; Rabalais et al., 2009), but also disproportionately increases respiration rates of heterotrophic organisms compared to oxygen production by primary producers.

In the Gulf, the increase of algae often aligns with the temperature rise (Fig. S7A). Chlorophyll-a concentration and chlorophyll fluorescence (i.e., band 678 nm used in this study) both have been widely used as the proxies of phytoplankton events (Jane et al., 2021; Scavia et al., 2017; Shen et al., 2019). Chlorophyll-a, specifically, is the primary type of chlorophyll present in green plants and algae, serving as an indicator to measure the abundance of phytoplankton in water bodies. Remote sensing reflectance at band 678 nm is often used for measuring normalized fluorescence line height (nflh) – a crucial indicator of the physiological status of phytoplankton (Behrenfeld et al., 2009), and it is also used in the Red Band Difference algorithms for detecting phytoplankton events (El-habashi et al., 2016). However, it is important to note that the nflh product has limitations and may be inaccurate in coastal waters, particularly in river-influenced areas where scattering is increased by the presence of non-algal particles (Bianchi et al., 2010; Gilerson et al., 2007; Walker and Rabalais, 2006). As algae exhibit a short life span, their growth and subsequent decay introduce substantial organic matter into the bottom water. The decomposition process by bacteria can, in turn, result in the depletion of oxygen (Fig. S1). This mechanism is supported by our findings, which show that proxies of phytoplankton events were important for modeling hypoxia.

Furthermore, heterotrophic respiration in both pelagic and benthic domains also plays a critical part in oxygen depletion. Elevated temperatures accelerate metabolic processes, leading to heightened bacterial degradation of organic matter and increased sediment oxygen consumption (Henson et al., 2013; Kim et al., 2023; Vázquez-Domínguez et al., 2007). Additionally, the imbalance between photosynthesis and respiration becomes more pronounced under warming, as heterotrophic processes are generally more temperature-sensitive than autotrophic ones. This imbalance, coupled with higher grazing rates by zooplankton, intensifies top-down control on phytoplankton biomass, further shifting the balance toward oxygen depletion (Kralj et al., 2019; O'Connor et al., 2009).

Water stratification due to warming makes dead zones worse by preventing water mixing that oxygenates water at lower depths (Fig. S1). The three water stratification-related variables – temperature difference between surface and bottom, salinity, and velocity – are also among the top twelve most important predictors (Fig. 4B). Other potential factors such as water residence time and circulation also significantly influence oxygen dynamics. Prolonged residence time and reduced circulation enhance stratification, limiting oxygen replenishment in bottom waters and compounding the effects of eutrophication. Future studies can further incorporate process-based models to provide a more comprehensive understanding of the mechanisms driving hypoxia, particularly in the context of a warming climate.

We did not include nutrient concentration or load as predictors in our model for two reasons: (1) the lack of spatial information on nutrient concentration in the coastal water; (2) there exists a strong lagged correlation ($r = 0.60 \pm 0.15$, $p < 0.001$) between nutrient loads to the Gulf and the chlorophyll-a levels (Fig. S7B) (Walker and Rabalais, 2006), but

the latter is a more direct driver of coastal water hypoxia and has spatial information from the satellite.

4.3. Knowledge gap in long-term global studies on dead zones and metacoupled land-ocean systems

In addition to the Gulf of Mexico, the UNEP, and the Intergovernmental Oceanographic Commission have identified 65 large marine coastal ecosystems across the globe that experienced similar human and natural stressors. Degradation of these ecosystems may result in interconnected and cumulative environmental effects, posing severe consequences on human well-being (UNEP-DHI and UNEP, 2016). To address these widespread challenges, there is an urgent need for long-term, global-scale, and consistent coastal monitoring efforts. Our model is a reproducible approach, employing freely available remotely sensed data and open-source algorithms on the GEE cloud computing platform, and can be adapted for use in other coastal ecosystems worldwide.

Our study also provides a foundation for using system thinking approaches when examining the linkages between large river basins and the adjacent coastal ecosystems (Best, 2019; Breitburg et al., 2018), especially the ones that have undergone severe impacts of dead zones (e.g., the East China Sea, the Black Sea, and the Gulf of Oman). While our approach is not explicitly designed to guide decision-making toward achieving the 5000 km^2 reduction target, it offers valuable insights for understanding hypoxia dynamics, informing processes, and exploring potential solutions. Coastal eutrophication leading to harmful dead zones is primarily driven by human pollution from terrestrial ecosystems, particularly agricultural activities such as fertilizer application and animal manure management. The metacoupling framework, which examines socio-environmental interactions within as well as between adjacent and distant systems, provides a valuable approach for linking nutrient contributions from regions within a watershed to hypoxia issues in distant coastal areas (Li et al., 2023a; Liu, 2023). Understanding these connections can improve insights into the timing and magnitude of nutrient delivery to coastal areas, facilitating the development of integrated policies and strategies to address nutrient reduction and mitigate coastal dead zones effectively.

Projections indicate that climate change and the expanding global population will amplify the spatial extent, duration, and intensity of global dead zones (Fennel and Testa, 2019; IOC-UNESCO and UNEP, 2016; Sinha et al., 2017). Improving the understanding of both historical and future dead zone dynamics under climate change is urgently needed to support early conservation efforts (Domínguez-Tejo et al., 2016; Ménesguen and Lacroix, 2018) and to advance progress toward the United Nations Sustainable Development Goals (SDGs)—particularly SDG 14, which focuses on the sustainable management and protection of marine and coastal ecosystems. Policy strategies like the Gulf Hypoxia Task Force could be one of the promising means of intervention to reduce fertilizer runoff and alleviate the dead zone consequences, however, their success depends on routine monitoring of both dead zone dynamics and policy effectiveness. Our study demonstrated that remote sensing could help track the spatiotemporal variation of large-scale coastal systems in combination with traditional in-situ field measurements. Future studies can leverage the methodology we developed for the Gulf of Mexico to expand our model to other regions. This will enable the prediction of future trends of coastal dead zones across space and time, enhancing insights for more informed coastal ecosystem assessments and management.

CRediT authorship contribution statement

Yingjie Li: Writing – review & editing, Writing – original draft, Visualization, Methodology, Investigation, Formal analysis, Data curation, Conceptualization. **Zilong Xia:** Writing – review & editing, Methodology, Investigation, Formal analysis. **Lan Nguyen:** Writing – review & editing, Methodology. **Ho Yi Wan:** Writing – review & editing, Methodology. **Luwen Wan:** Writing – review & editing, Methodology, Conceptualization. **Mengqiu Wang:** Writing – review & editing, Methodology. **Nan Jia:** Writing – review & editing, Methodology. **Venkata Rohith Reddy Matli:** Writing – review & editing, Methodology, Data curation. **Yi Li:** Writing – review & editing, Methodology. **Megan Seeley:** Writing – review & editing, Methodology. **Emilio F. Moran:** Writing – review & editing, Resources. **Jianguo Liu:** Writing – review & editing, Validation, Supervision, Resources, Funding acquisition, Conceptualization.

Declaration of competing interest

The authors declare that they have no known competing financial interests or personal relationships that could have appeared to influence the work reported in this paper.

Acknowledgements

We thank Annie Cooper Smith, Scott Swinton and Anthony Kendall for their valuable comments on the manuscript. This work received support from the NSF (DEB-1924111, OAC-2118329) and the Summer Research Fellowship by the Environmental Science and Policy Program. Support for this research was also provided by the NSF Long-term Ecological Research Program (DEB 2224712) at the Kellogg Biological Station and by Michigan State University AgBioResearch.

Code availability

Codes used for conducting the analyses are available at https://github.com/Yingjie4Science/dead-zone-mapping-from-satellite.

Data availability

The complete raw water sample data were provided by Venkata Rohith Reddy Matli and are currently unavailable to the public due to restrictions from the data holders. However, portions of the included data can be accessed from public sources, such as the National Oceanic and Atmospheric Administration (NOAA) National Centers for Environmental Information (https://www.ncei.noaa.gov/products/gulf-mexico-hypoxia-watch). All the satellite-derived data used in this study are publicly available, with sources and links provided in Table 1. The data from results used for producing figures in the manuscript are available at https://github.com/Yingjie4Science/dead-zone-mapping-from-satellite.

Appendix A. Supplementary data

Supplementary data to this article can be found online at https://doi.org/10.1016/j.scitotenv.2025.179461.

Data availability

Data will be made available on request.

References

Allahdadi, M.N., Jose, F., Patin, C., 2013. Seasonal hydrodynamics along the Louisiana coast: implications for hypoxia spreading. J. Coast. Res. 29, 1092–1100. https://doi.org/10.2112/JCOASTRES-D-11-00122.1.

Altieri, A.H., Gedan, K.B., 2015. Climate change and dead zones. Glob. Chang. Biol. 21, 1395–1406. https://doi.org/10.1111/gcb.12754.

Behrenfeld, M.J., Westberry, T.K., Boss, E.S., O'Malley, R.T., Siegel, D.A., Wiggert, J.D., Franz, B.A., McClain, C.R., Feldman, G.C., Doney, S.C., Moore, J.K., Dall'Olmo, G., Milligan, A.J., Lima, I., Mahowald, N., 2009. Satellite-detected fluorescence reveals global physiology of ocean phytoplankton. Biogeosciences 6, 779–794. https://doi.org/10.5194/bg-6-779-2009.

Belgiu, M., Drăguț, L., 2016. Random forest in remote sensing: a review of applications and future directions. ISPRS J. Photogramm. Remote Sens. 114, 24–31. https://doi.org/10.1016/j.isprsjprs.2016.01.011.

Best, J., 2019. Anthropogenic stresses on the world's big rivers. Nat. Geosci. 12, 7–21. https://doi.org/10.1038/s41561-018-0262-x.
Bianchi, T.S., DiMarco, S.F., Cowan, J.H., Hetland, R.D., Chapman, P., Day, J.W., Allison, M.A., 2010. The science of hypoxia in the northern Gulf of Mexico: a review. Sci. Total Environ. 408, 1471–1484. https://doi.org/10.1016/j.scitotenv.2009.11.047.
Boyce, D.G., Lewis, M., Worm, B., 2012. Integrating global chlorophyll data from 1890 to 2010. Limnol. Oceanogr. Methods 10, 840–852. https://doi.org/10.4319/lom.2012.10.840.
Breitburg, D., Levin, L.A., Oschlies, A., Grégoire, M., Chavez, F.P., Conley, D.J., Garçon, V., Gilbert, D., Gutiérrez, D., Isensee, K., Jacinto, G.S., Limburg, K.E., Montes, I., Naqvi, S.W.A., Pitcher, G.C., Rabalais, N.N., Roman, M.R., Rose, K.A., Seibel, B.A., Telszewski, M., Yasuhara, M., Zhang, J., 2018. Declining oxygen in the global ocean and coastal waters. Science 359, eaam7240. https://doi.org/10.1126/science.aam7240.
Brush, M.J., Giani, M., Totti, C., Testa, J.M., Faganeli, J., Ogrinc, N., Kemp, W.M., Umani, S.F., 2020. Eutrophication, harmful algae, oxygen depletion, and acidification. In: Coastal Ecosystems in Transition. American Geophysical Union (AGU), pp. 75–104. https://doi.org/10.1002/9781119543626.ch5.
Campbell, L.G., Thrash, J.C., Rabalais, N.N., Mason, O.U., 2019. Extent of the annual Gulf of Mexico hypoxic zone influences microbial community structure. PLoS One 14, e0209055. https://doi.org/10.1371/journal.pone.0209055.
Carstensen, J., Andersen, J.H., Gustafsson, B.G., Conley, D.J., 2014. Deoxygenation of the Baltic Sea during the last century. Proc. Natl. Acad. Sci., 201323156 https://doi.org/10.1073/pnas.1323156111.
Chen, C.-C., Gong, G.-C., Shiah, F.-K., 2007. Hypoxia in the East China Sea: one of the largest coastal low-oxygen areas in the world. Mar. Environ. Res. 64, 399–408. https://doi.org/10.1016/j.marenvres.2007.01.007.
Chen, Jianyu, Ni, X., Liu, M., Chen, Jianfang, Mao, Z., Jin, H., Pan, D., 2014. Monitoring the occurrence of seasonal low-oxygen events off the Changjiang estuary through integration of remote sensing, buoy observations, and modeling. J. Geophys. Res. Oceans 119, 5311–5322. https://doi.org/10.1002/2014JC010333.
Chen, S., Hu, C., Barnes, B.B., Xie, Y., Lin, G., Qiu, Z., 2019. Improving ocean color data coverage through machine learning. Remote Sens. Environ. 222, 286–302. https://doi.org/10.1016/j.rse.2018.12.023.
Conley, D.J., Carstensen, J., Aigars, J., Axe, P., Bonsdorff, E., Eremina, T., Haahti, B.-M., Humborg, C., Jonsson, P., Kotta, J., Lännegren, C., Larsson, U., Maximov, A., Medina, M.R., Lysiak-Pastuszak, E., Remeikaitė-Nikienė, N., Walve, J., Wilhelms, S., Zillén, L., 2011. Hypoxia is increasing in the coastal zone of the Baltic Sea. Environ. Sci. Technol. 45, 6777–6783. https://doi.org/10.1021/es201212r.
Cummings, J.A., Smedstad, O.M., 2013. Variational data assimilation for the global ocean. In: Data Assimilation for Atmospheric, Oceanic and Hydrologic Applications, II. Springer, pp. 303–343.
Dagg, M.J., Breed, G.A., 2003. Biological effects of Mississippi River nitrogen on the northern Gulf of Mexico—a review and synthesis. J. Mar. Syst. 43, 133–152. https://doi.org/10.1016/j.jmarsys.2003.09.002.
Del Giudice, D., Matli, V.R.R., Obenour, D.R., 2020. Bayesian mechanistic modeling characterizes Gulf of Mexico hypoxia: 1968–2016 and future scenarios. Ecol. Appl. 30, e02032. https://doi.org/10.1002/eap.2032.
Diaz, R.J., Rosenberg, R., 2008. Spreading dead zones and consequences for marine ecosystems. Science 321, 926–929. https://doi.org/10.1126/science.1156401.
Domínguez-Tejo, E., Metternicht, G., Johnston, E., Hedge, L., 2016. Marine spatial planning advancing the ecosystem-based approach to coastal zone management: a review. Mar. Policy 72, 115–130. https://doi.org/10.1016/j.marpol.2016.06.023.
Druon, J.N., Schrimpf, W., Dobricic, S., Stips, A., 2004. Comparative Assessment of Large-Scale Marine Eutrophication: North Sea Area and Adriatic Sea as Case Studies. Marine Ecology Progress Series.
El-habashi, A., Ioannou, I., Tomlinson, M.C., Stumpf, R.P., Ahmed, S., 2016. Satellite retrievals of Karenia brevis harmful algal blooms in the West Florida shelf using neural networks and comparisons with other techniques. Remote Sens. 8, 377. https://doi.org/10.3390/rs8050377.
Falcone, J.A., 2021. Estimates of County-Level Nitrogen and Phosphorus from Fertilizer and Manure from 1950 through 2017 in the Conterminous United States (Report No. 2020–1153), Open-File Report.. Reston, VA. https://doi.org/10.3133/ofr20201153.
Feng, Y., DiMarco, S.F., Jackson, G.A., 2012. Relative role of wind forcing and riverine nutrient input on the extent of hypoxia in the northern Gulf of Mexico. Geophys. Res. Lett. 39. https://doi.org/10.1029/2012GL051192.
Fennel, K., Testa, J.M., 2019. Biogeochemical controls on coastal hypoxia. Annu. Rev. Mar. Sci. 11, 105–130. https://doi.org/10.1146/annurev-marine-010318-095138.
Fennel, K., Laurent, A., Hetland, R., Justić, D., Ko, D.S., Lehrter, J., Murrell, M., Wang, L., Yu, L., Zhang, W., 2016. Effects of model physics on hypoxia simulations for the northern Gulf of Mexico: a model intercomparison. J. Geophys. Res. Oceans 121, 5731–5750. https://doi.org/10.1002/2015JC011577.
Forrest, D.R., Hetland, R.D., DiMarco, S.F., 2011. Multivariable statistical regression models of the areal extent of hypoxia over the Texas–Louisiana continental shelf. Environ. Res. Lett. 6, 045002. https://doi.org/10.1088/1748-9326/6/4/045002.
GEBCO, 2019. The GEBCO_2019 Grid—A Continuous Terrain Model of the Global Oceans and Land. Liverpool, UK, British Oceanographic Data Centre, National Oceanography Centre, NERC.
Gilerson, A., Zhou, J., Hlaing, S., Ioannou, I., Schalles, J., Gross, B., Moshary, F., Ahmed, S., 2007. Fluorescence component in the reflectance spectra from coastal waters. Dependence on water composition. Optics Express 15, 15702–15721. https://doi.org/10.1364/OE.15.015702.
Gorelick, N., Hancher, M., Dixon, M., Ilyushchenko, S., Thau, D., Moore, R., 2017. Google earth engine: planetary-scale geospatial analysis for everyone. Remote Sensing of Environment, Big Remotely Sensed Data: tools, applications and experiences 202, 18–27. https://doi.org/10.1016/j.rse.2017.06.031.
Greene, R.M., Lehrter, J.C., Iii, J.D.H., 2009. Multiple regression models for hindcasting and forecasting midsummer hypoxia in the Gulf of Mexico. Ecol. Appl. 19, 1161–1175. https://doi.org/10.1890/08-0035.1.
Harvey, E.T., Kratzer, S., Philipson, P., 2015. Satellite-based water quality monitoring for improved spatial and temporal retrieval of chlorophyll-a in coastal waters. Remote Sens. Environ. 158, 417–430. https://doi.org/10.1016/j.rse.2014.11.017.
Henson, S., Cole, H., Beaulieu, C., Yool, A., 2013. The impact of global warming on seasonality of ocean primary production. Biogeosciences 10, 4357–4369. https://doi.org/10.5194/bg-10-4357-2013.
Ho, J.C., Michalak, A.M., Pahlevan, N., 2019. Widespread global increase in intense lake phytoplankton blooms since the 1980s. Nature 1–17. https://doi.org/10.1038/s41586-019-1648-7.
Huang, R., Zhu, J., 2013. Using Random Forest to integrate lidar data and hyperspectral imagery for land cover classification. In: 2013 IEEE International Geoscience and Remote Sensing Symposium - IGARSS. Presented at the 2013 IEEE International Geoscience and Remote Sensing Symposium - IGARSS, pp. 3978–3981. https://doi.org/10.1109/IGARSS.2013.6723704.
Hutengs, C., Vohland, M., 2016. Downscaling land surface temperatures at regional scales with random forest regression. Remote Sens. Environ. 178, 127–141. https://doi.org/10.1016/j.rse.2016.03.006.
IOC-UNESCO, U.N.E., UNEP, U, 2016. Transboundary waters assessment Programme (TWAP). In: Large Marine Ecosystems: Status and Trends - Summary for Policy Makers, 4.
IPBES, 2019. Global assessment report on biodiversity and ecosystem services of the intergovernmental science-policy platform on biodiversity and ecosystem services. Zenodo. https://doi.org/10.5281/zenodo.3831674.
Jane, S.F., Hansen, G.J.A., Kraemer, B.M., Leavitt, P.R., Mincer, J.L., North, R.L., Pilla, R. M., Stetler, J.T., Williamson, C.E., Woolway, R.I., Arvola, L., Chandra, S., DeGasperi, C.L., Diemer, L., Dunalska, J., Erina, O., Flaim, G., Grossart, H.-P., Hambright, K.D., Hein, C., Hejzlar, J., Janus, L.L., Jenny, J.-P., Jones, J.R., Knoll, L. B., Leoni, B., Mackay, E., Matsuzaki, S.-I.S., McBride, C., Müller-Navarra, D.C., Paterson, A.M., Pierson, D., Rogora, M., Rusak, J.A., Sadro, S., Saulnier-Talbot, E., Schmid, M., Sommaruga, R., Thiery, W., Verburg, P., Weathers, K.C., Weyhenmeyer, G.A., Yokota, K., Rose, K.C., 2021. Widespread deoxygenation of temperate lakes. Nature 594, 66–70. https://doi.org/10.1038/s41586-021-03550-y.
Justić, D., Rabalais, N.N., Eugene Turner, R., Wiseman, W.J., 1993. Seasonal coupling between riverborne nutrients, net productivity and hypoxia. Mar. Pollut. Bull. 26, 184–189. https://doi.org/10.1016/0025-326X(93)90620-Y.
Justić, D., Rose, K.A., Hetland, R.D., Fennel, K., 2017. Modeling Coastal Hypoxia: Numerical Simulations of Patterns, Controls and Effects of Dissolved Oxygen Dynamics. Springer International Publishing. https://doi.org/10.1007/978-3-319-54571-4.
Kim, H.H., Laufkötter, C., Lovato, T., Doney, S.C., Ducklow, H.W., 2023. Projected 21st-century changes in marine heterotrophic bacteria under climate change. Front. Microbiol. 14. https://doi.org/10.3389/fmicb.2023.1049579.
Kim, Y.H., Son, S., Kim, H.-C., Kim, B., Park, Y.-G., Nam, J., Ryu, J., 2020. Application of satellite remote sensing in monitoring dissolved oxygen variabilities: a case study for coastal waters in Korea. Environ. Int. 134, 105301. https://doi.org/10.1016/j.envint.2019.105301.
Klemas, V., 2011. Remote sensing of algal blooms: an overview with case studies. J. Coast. Res. 34–43. https://doi.org/10.2112/JCOASTRES-D-11-00051.1.
Kralj, M., Lipizer, M., Čermelj, B., Celio, M., Fabbro, C., Brunetti, F., Francé, J., Mozetič, P., Giani, M., 2019. Hypoxia and dissolved oxygen trends in the northeastern Adriatic Sea (gulf of Trieste). Deep Sea research part II: topical studies in oceanography, revisiting the eastern Mediterranean: recent knowledge on the physical, biogeochemical and ecosystemic states and trends (volume I) 164, 74–88. doi:https://doi.org/10.1016/j.dsr2.2019.06.002.
Laurent, A., Fennel, K., 2019. Time-evolving, spatially explicit forecasts of the northern Gulf of Mexico hypoxic zone. Environ. Sci. Technol. 53, 14449–14458. https://doi.org/10.1021/acs.est.9b05790.
Le, C., Lehrter, J.C., Hu, C., Murrell, M.C., Qi, L., 2014. Spatiotemporal chlorophyll-a dynamics on the Louisiana continental shelf derived from a dual satellite imagery algorithm. J. Geophys. Res. Oceans 119, 7449–7462. https://doi.org/10.1002/2014JC010084.
Le, C., Lehrter, J.C., Hu, C., Obenour, D.R., 2016. Satellite-based empirical models linking river plume dynamics with hypoxic area and volume. Geophys. Res. Lett. 43, 2693–2699. https://doi.org/10.1002/2015GL067521.
Leming, T.D., Stuntz, W.E., 1984. Zones of coastal hypoxia revealed by satellite scanning have implications for strategic fishing. Nature 310, 136–138. https://doi.org/10.1038/310136a0.
Li, Y., Jia, N., Yu, X., Manning, N., Lan, X., Liu, J., 2023a. Transboundary flows in the metacoupled Anthropocene: typology, methods, and governance for global sustainability. Ecol. Soc. 28. https://doi.org/10.5751/ES-14351-280319.
Li, Y., Robinson, S.V.J., Nguyen, L.H., Liu, J., 2023b. Satellite prediction of coastal hypoxia in the northern Gulf of Mexico. Remote Sens. Environ. 284, 113346. https://doi.org/10.1016/j.rse.2022.113346.
Limburg, K.E., Breitburg, D., Swaney, D.P., Jacinto, G., 2020. Ocean deoxygenation: a primer. One. Earth 2, 24–29. https://doi.org/10.1016/j.oneear.2020.01.001.
Lin, S., 2017. Climate change and algal blooms. Michigan State University, East Lansing. https://doi.org/10.25335/SQ1F-TF58.
Linderman, M.A., An, L., Bearer, S., He, G., Ouyang, Z., Liu, J., 2005. Modeling the spatio-temporal dynamics and interactions of households, landscapes, and giant panda habitat. Ecol. Model. 183, 47–65. https://doi.org/10.1016/j.ecolmodel.2004.07.026.

Lipizer, M., Partescano, E., Rabitti, A., Giorgetti, A., Crise, A., 2014. Qualified temperature, salinity and dissolved oxygen climatologies in a changing Adriatic Sea. Ocean Sci. 10, 771–797. https://doi.org/10.5194/os-10-771-2014.

Liu, J., 2023. Leveraging the metacoupling framework for sustainability science and global sustainable development. Natl. Sci. Rev. 10, nwad090. https://doi.org/10.1093/nsr/nwad090.

Matli, V.R.R., Fang, S., Guinness, J., Rabalais, N.N., Craig, J.K., Obenour, D.R., 2018. A space-time geostatistical assessment of hypoxia in the northern Gulf of Mexico. Environ. Sci. Technol. https://doi.org/10.1021/acs.est.8b03474.

Matli, V.R.R., Laurent, A., Fennel, K., Craig, K., Krause, J., Obenour, D.R., 2020. Fusion-based hypoxia estimates: combining geostatistical and mechanistic models of dissolved oxygen variability. Environ. Sci. Technol. https://doi.org/10.1021/acs.est.0c03655.

Ménesguen, A., Lacroix, G., 2018. Modelling the marine eutrophication: a review. Sci. Total Environ. 636, 339–354. https://doi.org/10.1016/j.scitotenv.2018.04.183.

Mitsch, W.J., Day, J.W., Gilliam, J.W., Groffman, P.M., Hey, D.L., Randall, G.W., Wang, N., 2001. Reducing nitrogen loading to the Gulf of Mexico from the Mississippi River basin: strategies to counter a persistent ecological problem. BioScience 51, 373–388. https://doi.org/10.1641/0006-3568(2001)051[0373:RNLTTG]2.0.CO;2.

Murphy, R.R., Kemp, W.M., Ball, W.P., 2011. Long-term trends in Chesapeake Bay seasonal hypoxia, stratification, and nutrient loading. Estuar. Coasts 34, 1293–1309. https://doi.org/10.1007/s12237-011-9413-7.

Murray, C.J., Muller-Karulis, B., Carstensen, J., Conley, D.J., Gustafsson, B., Andersen, J. H., 2019. Past, present and future eutrophication status of the Baltic Sea. Front. Mar. Sci. 6. https://doi.org/10.3389/fmars.2019.00002.

NOAA, 2022. NOAA forecasts summer "dead zone" of nearly 5.4K square miles in Gulf of Mexico [WWW document]. URL http://www.noaa.gov/news-release/noaa-forecasts-summer-dead-zone-of-nearly-54k-square-miles-in-gulf-of-mexico (accessed 7.31.22).

Obenour, D.R., Scavia, D., Rabalais, N.N., Turner, R.E., Michalak, A.M., 2013. Retrospective analysis of midsummer hypoxic area and volume in the northern Gulf of Mexico, 1985-2011. Environ. Sci. Technol. 47, 9808–9815. https://doi.org/10.1021/es400983g.

Obenour, D.R., Michalak, A.M., Scavia, D., 2015. Assessing biophysical controls on Gulf of Mexico hypoxia through probabilistic modeling. Ecol. Appl. 25, 492–505. https://doi.org/10.1890/13-2257.1.

O'Connor, M.I., Piehler, M.F., Leech, D.M., Anton, A., Bruno, J.F., 2009. Warming and resource availability shift food web structure and metabolism. PLoS Biol. 7, e1000178. https://doi.org/10.1371/journal.pbio.1000178.

Ou, Y., Xue, Z.G., 2024. Hydrodynamic and biochemical impacts on the development of hypoxia in the Louisiana–Texas shelf – Part 1: roles of nutrient limitation and plankton community. Biogeosciences 21, 2385–2424. https://doi.org/10.5194/bg-21-2385-2024.

Pelletier, C., Valero, S., Inglada, J., Champion, N., Dedieu, G., 2016. Assessing the robustness of random forests to map land cover with high resolution satellite image time series over large areas. Remote Sens. Environ. 187, 156–168. https://doi.org/10.1016/j.rse.2016.10.010.

Pitcher, G.C., Aguirre-Velarde, A., Breitburg, D., Cardich, J., Carstensen, J., Conley, D.J., Dewitte, B., Engel, A., Espinoza-Morriberón, D., Flores, G., Garçon, V., Graco, M., Grégoire, M., Gutiérrez, D., Martin Hernandez-Ayon, J., May Huang, H.-H., Isensee, K., Elena Jacinto, M., Levin, L., Lorenzo, A., Machu, E., Merma, L., Montes, I., Swa, N., Paulmier, A., Roman, M., Rose, K., Hood, R., Rabalais, N.N., Gro V. Salvanves, A., Salvatteci, R., Sánchez, S., Sifeddine, A., Wahab Tall, A., van der Plas, A.K., Yasuhara, M., Zhang, J., Zhu, Z., 2021. System controls of coastal and open ocean oxygen depletion. Prog. Oceanogr. 102613. https://doi.org/10.1016/j.pocean.2021.102613.

Rabalais, N.N., Turner, R.E., 2019. Gulf of Mexico hypoxia: past, present, and future. Limnology and Oceanography Bulletin 28, 117–124. https://doi.org/10.1002/lob.10351.

Rabalais, N.N., Turner, R.E., Díaz, R.J., Justić, D., 2009. Global change and eutrophication of coastal waters. ICES J. Mar. Sci. 66, 1528–1537. https://doi.org/10.1093/icesjms/fsp047.

Rabalais, N.N., Díaz, R.J., Levin, L.A., Turner, R.E., Gilbert, D., Zhang, J., 2010. Dynamics and distribution of natural and human-caused hypoxia. Biogeosciences 7, 585–619. https://doi.org/10.5194/bg-7-585-2010.

Rabotyagov, S.S., Kling, C.L., Gassman, P.W., Rabalais, N.N., Turner, R.E., 2014. The economics of dead zones: causes, impacts, policy challenges, and a model of the Gulf of Mexico hypoxic zone. Rev. Environ. Econ. Policy 8, 58–79. https://doi.org/10.1093/reep/ret024.

Rodriguez-Galiano, V.F., Ghimire, B., Rogan, J., Chica-Olmo, M., Rigol-Sanchez, J.P., 2012. An assessment of the effectiveness of a random forest classifier for land-cover classification. ISPRS J. Photogramm. Remote Sens. 67, 93–104. https://doi.org/10.1016/j.isprsjprs.2011.11.002.

Rubí, J.N.S., de Carvalho, P.H.P., Gondim, P.R.L., 2023. Application of machine learning models in the behavioral study of forest fires in the Brazilian Federal District region. Eng. Appl. Artif. Intell. 118, 105649. https://doi.org/10.1016/j.engappai.2022.105649.

Scavia, D., Evans, M.A., Obenour, D.R., 2013. A scenario and forecast model for Gulf of Mexico hypoxic area and volume. Environ. Sci. Technol. 47, 10423–10428. https://doi.org/10.1021/es4025035.

Scavia, D., Bertani, I., Obenour, D.R., Turner, R.E., Forrest, D.R., Katin, A., 2017. Ensemble modeling informs hypoxia management in the northern Gulf of Mexico. Proc. Natl. Acad. Sci. 114, 8823–8828. https://doi.org/10.1073/pnas.1705293114.

Shao, Z., Cai, J., Fu, P., Hu, L., Liu, T., 2019. Deep learning-based fusion of Landsat-8 and Sentinel-2 images for a harmonized surface reflectance product. Remote Sens. Environ. 235, 111425. https://doi.org/10.1016/j.rse.2019.111425.

Shen, F., Tang, R., Sun, X., Liu, D., 2019. Simple methods for satellite identification of algal blooms and species using 10-year time series data from the East China Sea. Remote Sens. Environ. 235, 111484. https://doi.org/10.1016/j.rse.2019.111484.

Sinha, E., Michalak, A.M., Balaji, V., 2017. Eutrophication will increase during the 21st century as a result of precipitation changes. Science 357, 405–408. https://doi.org/10.1126/science.aan2409.

Smith, M.D., Oglend, A., Kirkpatrick, A.J., Asche, F., Bennear, L.S., Craig, J.K., Nance, J. M., 2017. Seafood prices reveal impacts of a major ecological disturbance. Proc. Natl. Acad. Sci. 201617948. https://doi.org/10.1073/pnas.1617948114.

Teluguntla, P., Thenkabail, P.S., Oliphant, A., Xiong, J., Gumma, M.K., Congalton, R.G., Yadav, K., Huete, A., 2018. A 30-m landsat-derived cropland extent product of Australia and China using random forest machine learning algorithm on Google earth engine cloud computing platform. ISPRS J. Photogramm. Remote Sens. 144, 325–340. https://doi.org/10.1016/j.isprsjprs.2018.07.017.

Tomasetti, S.J., Gobler, C.J., 2020. Dissolved oxygen and pH criteria leave fisheries at risk. Science 368, 372–373. https://doi.org/10.1126/science.aba4896.

Turner, R.E., Rabalais, N.N., Justić, D., 2012. Predicting summer hypoxia in the northern Gulf of Mexico: redux. Mar. Pollut. Bull. 64, 319–324. https://doi.org/10.1016/j.marpolbul.2011.11.008.

Turner, R.E., Rabalais, N.N., Glaspie, C.N., 2024. A temperature tipping point in hypoxic zone size. Limnol. Oceanogr. 69, 2954–2962. https://doi.org/10.1002/lno.12722.

UNEP-DHI, U.N.E., UNEP, U.N.E, 2016. Transboundary River Basins: Status and Trends. Summary for Policy Makers, United Nations Environment Programme (UNEP), Nairobi.

US EPA, 2008. Gulf Hypoxia Action Plan 2008 for Reducing, Mitigating, and Controlling Hypoxia in the Northern Gulf of Mexico and Improving Water Quality in the Mississippi River Basin. Washington, DC.

US EPA, 2023. Mississippi River/Gulf of Mexico Watershed Nutrient Task Force: 2023 Report to Congress (Reports and Assessments).

Vázquez-Domínguez, E., Vaqué, D., Gasol, J.M., 2007. Ocean warming enhances respiration and carbon demand of coastal microbial plankton. Glob. Chang. Biol. 13, 1327–1334. https://doi.org/10.1111/j.1365-2486.2007.01377.x.

Walker, N.D., Rabalais, N.N., 2006. Relationships among satellite chlorophyll a, river inputs, and hypoxia on the Louisiana continental shelf, Gulf of Mexico. Estuar. Coasts 29, 1081–1093. https://doi.org/10.1007/bf02781811.

Wang, L., Justić, D., 2009. A modeling study of the physical processes affecting the development of seasonal hypoxia over the inner Louisiana-Texas shelf: circulation and stratification. Cont. Shelf Res. 29, 1464–1476. https://doi.org/10.1016/j.csr.2009.03.014.

Wood, S.N., Bravington, M.V., Hedley, S.L., 2008. Soap film smoothing. J. R. Stat. Soc. Ser. B Stat Methodol. 70, 931–955. https://doi.org/10.1111/j.1467-9868.2008.00665.x.

Xia, Z., Li, Y., Chen, R., Sengupta, D., Guo, X., Xiong, B., Niu, Y., 2022. Mapping the rapid development of photovoltaic power stations in northwestern China using remote sensing. Energy Rep. 8, 4117–4127. https://doi.org/10.1016/j.egyr.2022.03.039.

You, N., Dong, J., Huang, J., Du, G., Zhang, G., He, Y., Yang, T., Di, Y., Xiao, X., 2021. The 10-m crop type maps in Northeast China during 2017–2019. Scientific Data 8, 41. https://doi.org/10.1038/s41597-021-00827-9.

Zhou, F., Chai, F., Huang, D., Wells, M., Ma, X., Meng, Q., Xue, H., Xuan, J., Wang, P., Ni, X., Zhao, Q., Liu, C., Su, J., Li, H., 2020. Coupling and decoupling of high biomass phytoplankton production and hypoxia in a highly dynamic coastal system: the Changjiang (Yangtze River) estuary. Front. Mar. Sci. 7.

Zhou, Y., Scavia, D., Michalak, A.M., 2014. Nutrient loading and meteorological conditions explain interannual variability of hypoxia in Chesapeake Bay. Limnol. Oceanogr. 59, 373–384. https://doi.org/10.4319/lo.2014.59.2.0373.

Zhu, Z.-Y., Zhang, J., Wu, Y., Zhang, Y.-Y., Lin, J., Liu, S.-M., 2011. Hypoxia off the Changjiang (Yangtze River) estuary: oxygen depletion and organic matter decomposition. Mar. Chem. 125, 108–116. https://doi.org/10.1016/j.marchem.2011.03.005.